Bioconjugate Chemistry

Article

12b80 - Hydroxybisphosphonate linked doxorubicin: bone targeted strategy for treatment of osteosarcoma

Emmanuelle David, Sébastien Cagnol, Jean-Yves Goujon, Maxim Egorov, Julien Taurelle, Charlène Benesteau, Laëtitia Morandeau, Christelle Moal, Marie Sicard, Samuel Pairel, Dominique Heymann, Francoise Redini, François Gouin, and Ronan Le Bot

Bioconjugate Chem., **Just Accepted Manuscript** • DOI: 10.1021/acs.bioconjchem.9b00210 • Publication Date (Web): 02 May 2019

ACS Publications

is published by the American Chemical Society. 1155 Sixteenth Street N.W., Washington, DC 20036

TITLE
12b80 - Hydroxybisphosphonate linked doxorubicin: bone targeted strategy for treatment of osteosarcoma

AUTHOR NAMES
Emmanuelle David*°, Sébastien Cagnol°, Jean-Yves Goujon°, Maxim Egorov°, Julien Taurelle°, Charlène Benesteau°, Laëtitia Morandeau°, Christelle Moal°, Marie Sicard°, Samuel Pairel°, Dominique Heymann•, Françoise Redini$^{\Psi}$, François Gouin‡ and Ronan Le Bot°.

AUTHOR ADDRESS
°Atlanthera, 3 rue Aronnax, 44821 Saint Herblain, France. • Institut de Cancérologie de l'Ouest, Inserm, CRCINA, Université de Nantes, Université d'Angers. Blvd Jacques Monod, 44805 Saint-Herblain, France. $^{\Psi}$ INSERM UMR1238, Université de Nantes, Sarcomes osseux et remodelage des tissus calcifiés, Faculté de médecine, 44035 Nantes, France. ‡Departement de chirurgie, centre Léon Bérard, 28 rue Laënnec, 69008 Lyon, France.

KEYWORDS
bisphosphonates, bone targeting, doxorubicin, drug conjugation, drug delivery, osteosarcoma.

ABSTRACT: To reply to as yet unmet medical needs to treat osteosarcoma, a form of primary bone cancer, we conceived the 12b80 compound by covalently conjugating antineoplastic compound doxorubicin to a bone targeting hydroxybisphosphonate vector and turn it into a prodrug through a custom linker designed to specifically trigger doxorubicin release in acidic bone tumor microenvironment. Synthesis of 12b80 was thoroughly optimized to be produced at gram scale. 12b80 was evaluated *in-vitro* for high bone support affinity, specific release of doxorubicin in acidic condition, lower cytotoxicity and cellular uptake of the prodrug. *In-vivo* in rodents, 12b80 displayed rapid and sustained targeting of bone tissue and tumor-associated heterotopic bone and permitted a higher doxorubicin payload in tumor bone environment compared to non-vectorized doxorubicin. Consequently, 12b80 showed much less toxicity compared to doxorubicin, promoted strong antitumor effects on rodent orthotopic osteosarcoma, displayed a dose-response therapeutic effect and was more potent than doxorubicin/zoledronate combination.

INTRODUCTION

Osteosarcoma is the most common primary bone tumor, a rare form of cancer, which accounts for less than 0.2% of all cancers and represents less than 1500 and 1000 patients diagnosed each year respectively in Europe and USA[1,2]. Osteosarcoma can occur at any age but has a higher incidence in patients under 24, with a peak during pubertal growth around 15[3]. The disease has an early and highly invasive and distant metastatic risk (particularly to lungs) associated with a poor outcome. Although it can develop in any bone, 80% of osteosarcomas affect the bone tissue with rapid growth such as the extremities of long bones (femur, tibia, humerus). Osteosarcoma derives from osteoblasts and is characterized both by bone formation and osteolytic lesions. Indeed, tumor cells promote formation of tumor osteoid (immature bone tissue) and tumoral heterotopic bone tissue. In addition, osteosarcoma cancer cells activate osteoclasts leading to osteolysis (bone resorption) and acidic tumor microenvironment. Current strategy of treatment for osteosarcoma includes neoadjuvant chemotherapy, limb salvage surgery and adjuvant chemotherapy. The most effective chemotherapy regimen is the combination of doxorubicin, cisplatin and high-dose methotrexate (called MAP); etoposide or ifosfamide can also be used in addition[4,5]. Despite efforts to improve treatments, 5-year event-free survival (EFS) rates have remained below 70% for patients with localized tumors[6]. Prognosis is worse for patients with unresectable primary disease or metastatic disease with 5-year EFS rates around 30%[7,8]. Because the survival rates have not significantly changed in the past 30 years (10-year survival rate increased from only 57.7 to 61%[9]), new therapeutic approaches are needed. To reply to as yet unmet medical need, our rational was to covalently bind a bone targeting vector to a potent gold standard antineoplastic compound to bring and deliver it in higher quantity in tumor bone environment to improve efficacy and decrease systemic distribution and associated toxicity. Our proof of principle was demonstrated with 12b80: a cleavable hydroxybisphosphonate (HBP) bound doxorubicin. A HBP was chosen as the bone targeting vector thanks to its strong affinity to bone tissue[10,11]. Furthermore, HBPs have been used to treat bone metastasis malignancies and postmenopausal osteoporosis as a preventive therapy against skeletal-related events[12,13]. Some research was carried out to improve the systemic anticancer properties

of hydroxybisphosphonates themselves by masking the phosphonic acid through organic protecting groups and introducing hydrophobic functions in the side chain to reduce their polarity, osseous affinity and to improve the soft tissue uptake[14]. Structure-antitumor activity relationship investigation of non-protected hydroxybisphosphonates themselves resulted in compound showing *in-vitro* anti-proliferative activity against tumor cell lines with IC50 value of 9.5 x 10^{-5} M [15]. In the actual work doxorubicin was selected as an optimal antineoplastic agent to vectorize since it is considered as the gold standard in sarcoma therapy, including osteosarcoma, but shows a limited therapeutic index due to severe cardiac toxicity. Furthermore, we benefited from the natural fluorescence of doxorubicin due to its anthracycline chromophore group, to facilitate distribution study. The innovation of 12b80 lies in its customized linker designed to take advantage of the acidity of bone tumor microenvironment to specifically trigger the doxorubicin release. This linker also contributes considerably to the high hydrosolubility of 12b80. Bisphosphonate (BP) molecules have been studied extensively since the 1960's and a multitude of BP-based products are commercially available[16]. Mechanistically, BPs exhibit affinity toward bone by chelating calcium ions present in bone hydroxyapatite (HA). The involvement of phosphonate groups in the HA binding mechanism was further evaluated to investigate the effect of phospho-esters on the ability of the BP to bind HA[10]. One of the varieties of BP are HBPs having a hydroxyl group on the carbon atom of the BP moiety participating in the binding of these compounds to the mineralized bone matrix[17] and rising the affinity for HA crystals by tridentate binding[18]. For this reason, HBP vectors are more efficient for the bone targeting than BP. Classic methods of simple HBP compound synthesis were reviewed and are rather drastic to be convenient for multifunctional HBP molecule synthesis[19]. That is why only few attempts to synthetize complex individual bifunctional HBP molecules vectorizing a potent API are published. Such molecules have advantages of strictly defined chemical structure, API content, physicochemical characteristics and purity. Meanwhile the study of non-HBP polymer self-assembling nanoparticle delivery systems, vectorizing covalently bounded doxorubicin[20,21] and daunorubicin[22] led to improve their *in-vitro* efficacy. Redox tumor-sensitive non-HBP nanoparticle carrier for free methotrexate encapsulation has been reported[23]. For nanoparticles coated with HBP groups, the osseous affinity[24] and anticancer activity of supported doxorubicin[25] in the bone have been demonstrated. Development of bone targeting anticancer therapy is a promising strategy[26,27]. Some projects were conducted on bisphosphonate-conjugated antineoplastic agents but only few of them have shown evidence of antitumor activity in osteosarcoma models. The first one was based on HBP vectorized liposomes charged with non-modified doxorubicin[28]. The second one, the MBC-11 molecule which consists of the HBP etidronate conjugated to the antineoplastic agent cytarabine, has been tested clinically and was the first bisphosphonate conjugate to demonstrate efficacy in first-in-human phase I on cancer induced bone disease[29]. Furthermore, HBP-linked doxorubicin demonstrated efficacy in a model of bone metastases[30]. Those publications strongly support the interest of targeting bone tumor with HBP conjugated drugs and the need for new efficient synthetic approaches to the HBP bifunctional molecules. Most of the studies describing HBP- and BP-linked doxorubicin are based on synthetically more accessible BP vectors[31,32]. But even in these cases, only small amounts of final products were obtained, sometimes without pure final product isolation, and with rather low solubility (1-5 mM)[31] which was probably not sufficient for detailed physicochemical and biological property studies. Moreover, the use of the acid sensitive acylhydrazone linker is associated to a fast cleavage rate that could disadvantage prodrug safety and large scale chemical production. In contrast, we designed a thiocarbohydrazone type imine linker for 12b80 molecule to reduce systemic toxicity, to increase the aqueous solubility (up to 255 mM)[33] and to improve the stability during large scale production. The synthesis of 12b80 compound was thoroughly optimized to be produced at gram scale. Thus, the aim of this paper was to describe the improved synthesis of 12b80, its properties and its efficacy for the treatment of osteosarcoma.

RESULTS AND DISCUSSION

Synthesis and structure. Our previous approaches to the synthesis of various HBP-conjugated anticancer drugs showed that in the case of the doxorubicin, the aqueous solubility of the final HBP compound was limited[34]. Therefore, we designed new HBP conjugated doxorubicin molecules, for improvement of aqueous solubility[33] and succeeded in the **12b80** molecule. **12b80** molecule consists of three building blocks: the **Doxorubicin**, the **Linker** and the **HBP vector** conjugated together through imine bonds (Figure 1). The custom designed **Linker** played a key role in both acid sensitive doxorubicin release and high aqueous solubility of **12b80**. The synthesis of the **Vector** has been described previously[34]. Briefly, the 3-hydroxybenzaldehyde **1** was alkylated with 1,3-dibromopropane and the aldehyde group of **2** was protected with an acetal group to give the intermediate **3**. Substitution of bromine atom with methylamine followed by the Mikael addition of acrylic acid on **4** gave the acid **5**, the total yield was 65% over 4 steps. The conversion of the carboxyl of **5** to the HBP group was initially carried out using the mild catecholborane activation method[19,34–36] with highly nucleophilic tris(trimethylsilyl)phosphite[37]. Though this method is efficient, in the present work especially for the **Vector** we improved the yield of this step from 40% to 60% via the pivalic acid mixed anhydride method of HBP derivatives synthesis that we developed earlier[33]. This approach allowed also to bypass the chromatographic purification of the **Vector** and scale up the synthesis to 32 g of the final product. We reported the **Linker** synthesis starting from the anhydride **6** earlier[33]. In the present work we optimized its isolation procedure for the large-scale synthesis (up to 45 g) using original ethylene glycol/MeCN mixture that allowed to reach higher concentration and purity during **Linker** isolation step. Initially, **12b80** molecule was synthesized by a simultane-

ous coupling of the **Linker** to the **Doxorubicin** and the **Vector**[33]. To obtain a higher conversion of **Doxorubicin**, the synthesis was optimized: the **Linker-Vector** was first synthesized, which was thereafter coupled with the **Doxorubicin** resulting in at least 1.6 times higher yield and better reproducibility. Final **12b80** compound was obtained as a disodium salt readily soluble in the water. The structure of **12b80** molecule was proved by 1D and 2D NMR spectroscopy methods. The configurations of the imine bonds were proved by the NOEs analysis (Figure 2).

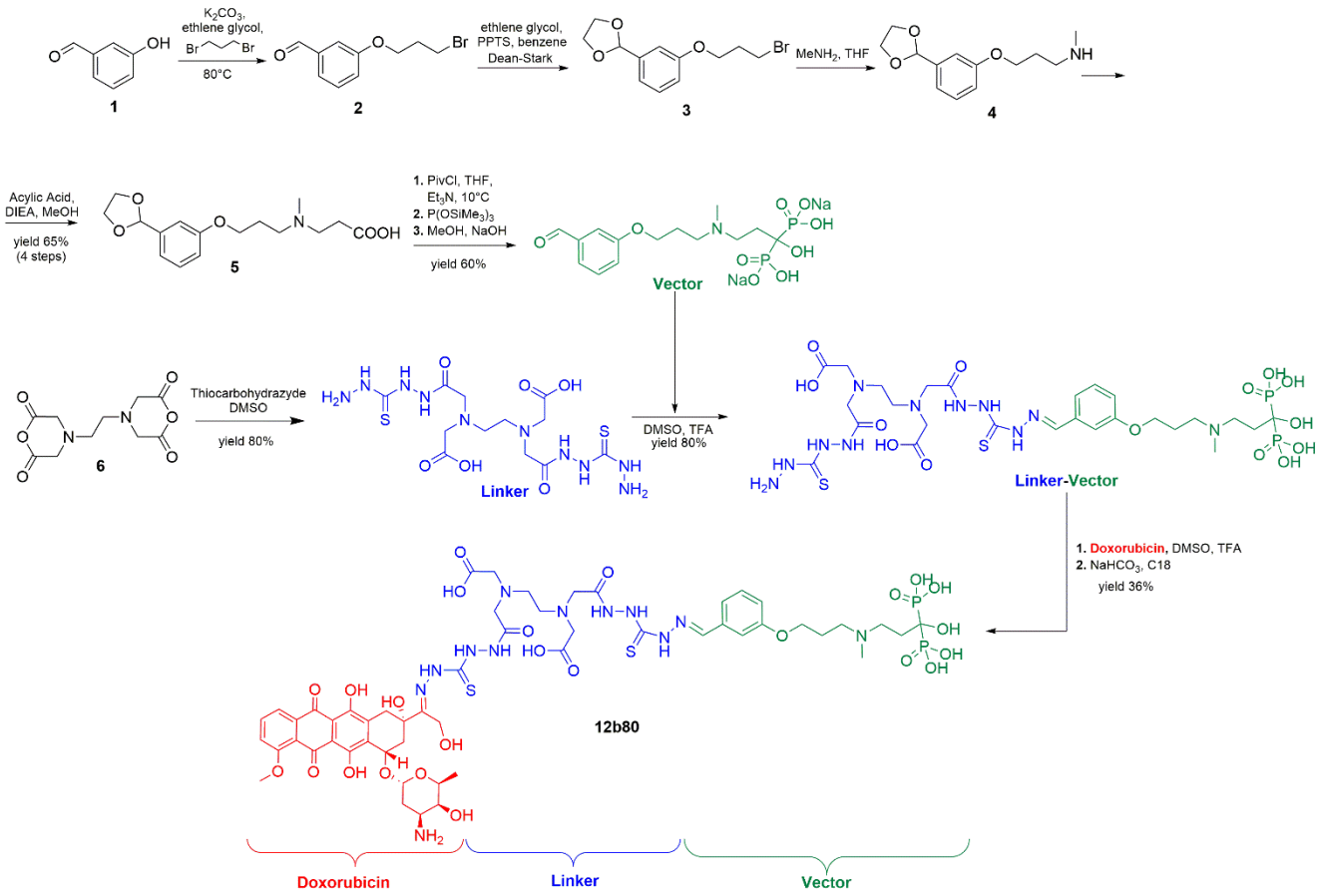

Figure 1. Optimized synthesis of the 12b80 molecule.

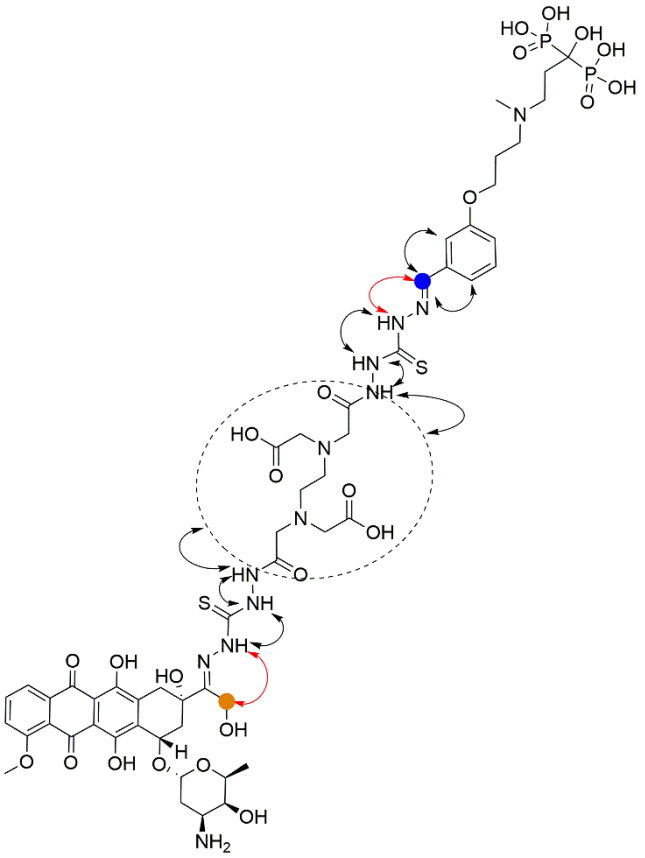

Figure 2. Key NOEs in the 12b80 molecule (NOESY, 1%TFA-D/DMSO-D_6, 400 MHz).

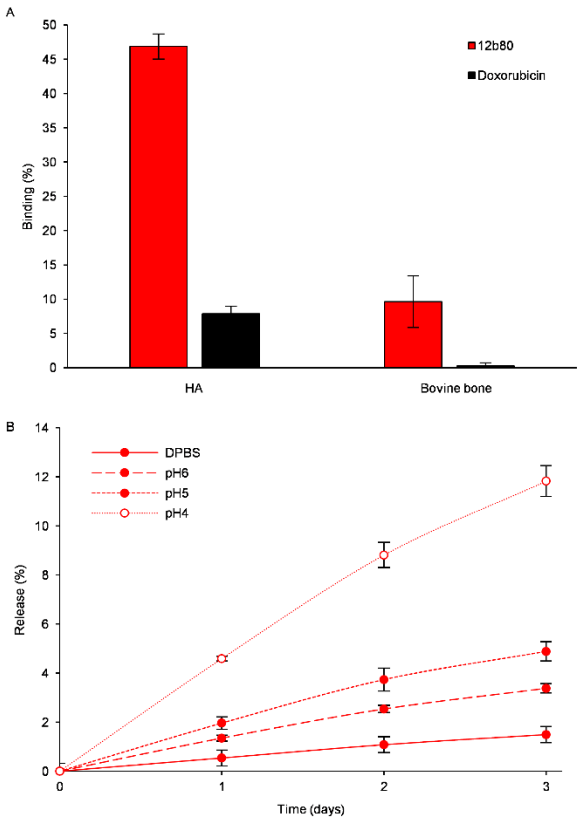

Figure 3: *In-vitro* binding and release of 12b80. A: Binding assay to hydroxyapatite (HA) and bovine bone. Rate of binding of 12b80 (red) and doxorubicin (black) on supports was determined by HPCL analysis of supernatant after 30 minutes of contact. Experiments were performed in triplicate and results are expressed in Mean ± SD. B: Tumor-associated acidic pH triggered doxorubicin release from 12b80. Doxorubicin release from hydroxyapatite-fixed 12b80 was studied in-vitro and measured by HPLC at 4 different pH: DPBS (pH 7.4) or citrate buffer (pH 6, 5, 4). Tumor-associated pH is ± 6 and tumor-associated osteolysis pH is ± 4

Binding of 12b80 to HA and bone. The binding of 12b80 was evaluated on 2 supports, HA and natural bovine bone, in comparison with doxorubicin. The rate of binding of 12b80 was respectively 47% and 10% on HA and bone within 30 minutes (Figure 3A). In comparison, the rate of binding of doxorubicin was respectively 8% and 0.3% on HA and bone. 12b80 exhibited rapid fixation and high affinity for synthetic and natural calcium phosphate compared to doxorubicin. These results were in accordance with published data on HBP affinity for HA[30,31].

Doxorubicin release from 12b80-HA at different pH medium. The release of doxorubicin from HA coated with 12b80 was investigated by HPLC in medium with different pH. As shown in Figure 3B, there was a direct relationship between acidity and release rate of doxorubicin. Less than 2% of doxorubicin was released from support within 3 days at a neutral pH (7.4: DPBS), in contrast, over 11% of doxorubicin was cleaved from 12b80 at the same time at a pH of 4. Intermediary release levels were observed at pH 5 and 6. Linker structure with imine bonds was indeed designed to be sensitive to low pH, to take advantage of the acidic pH associated with tumor cell microenvironment (pH between 6 and 7)[38,39] and with the osteoclast-associated bone resorptive activity pH in the range of 4[40]. *In-vitro* release studies with 12b80 highlighted the ability of acidic conditions associated with bone tumor to trigger the continuous release of doxorubicin from 12b80.

In-vitro cytotoxicity of 12b80. The effects of doxorubicin and 12b80 treatment on cell viability were compared *in-vitro* on normal mouse fibroblast L929 cells and on osteosarcoma-derived rat OSRGa cells after 72 h of treatment with doses ranging from 5 nM to 50 µM. As shown in Figure 4, IC50 of doxorubicin was around 134 nM in OSRGa cells and 239 nM in L929 cells, while IC50 of 12b80 was around 1.1 µM in OSRGa cells and 3.1 µM in L929 cells. Those results clearly indicated that 12b80 treatment was less toxic than non-vectorised doxorubicin, with a 8.3 fold higher and 12.9 fold higher IC50 for 12b80 in comparison to doxorubicin in cancerous OSRGa cells and fibroblast cells respectively. Those results supported the postulate that conjugation of doxorubicin to HBP vector through 12b80 molecule could turn doxorubicin into a less toxic prodrug.

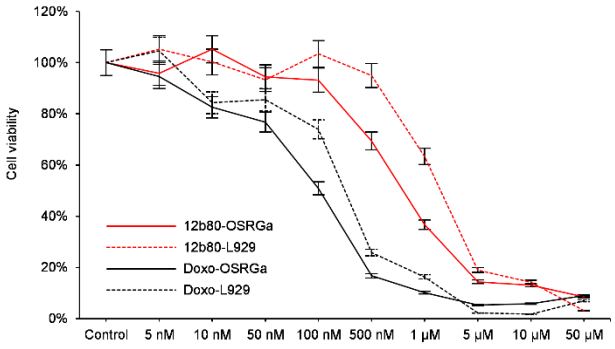

Figure 4: Comparison of doxorubicin and 12b80 treatments on cell viability. Exponentially growing immortalized fibroblastic mouse L929 cells or osteosarcoma-derived rat OSGRa cells were treated for 72 h with doxorubicin (Doxo), 12b80 or their respective solvent (control) at doses from 5 nM to 50 µM. Results represented as Mean ± SD of triplicats.

Cellular intake of 12b80 *in-vitro*. Analysis of intra cellular drug uptake in OSRGa cells by detection of doxorubicin-associated fluorescence showed that fluorescence associated with free doxorubicin started to be detectable 1 h after treatment to gradually increase in fluorescence intensity throughout the 48 h of treatment. Localization of the fluorescence signal was mostly in the nuclear compartment after 1 h and 4 h of treatment and delocalized from the nuclear to the peri-nuclear compartment after 8 h to be mostly localized at the periphery of nucleus after 24 h of treatment (Figure 5). Such cytosolic distribution of doxorubicin has previously been shown to be associated with P-Glycoprotein mediated drug resistance[41]. In contrast, uptake of 12b80-associated fluorescence started to be detectable after 8h of treatment. Fluorescence signal remained weak and only increased between 24 h and 48 h of treatment suggesting a lower cellular uptake of 12b80 in comparison with doxorubicin. Fluorescence signal associated with 12b80 was only detectable in the perinuclear compartment of cells. We postulated that perinuclear localization of 12b80 could be a hallmark of fluid phase endocytosis mechanism related to cellular entry of HBP molecules[42–44]. Since most of the proapoptotic effects of doxorubicin are associated with DNA damage, lower cell uptake and absence of detectable nuclear localization of 12b80 molecule could contribute to the lower *in-vitro* toxicity of HBP-conjugated doxorubicin prodrug.

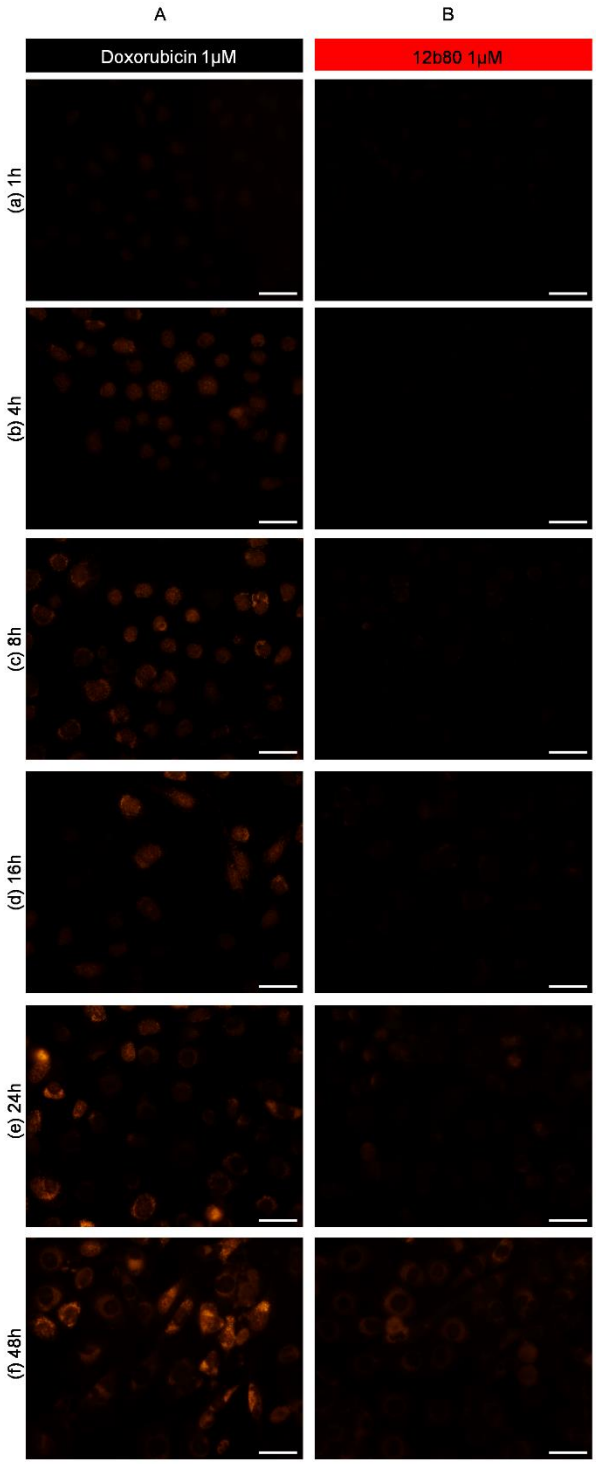

Figure 5: Comparison of doxorubicin and 12b80 cellular uptake and distribution. A: OSRGa cells have been treated with 1 µM doxorubicin for 1 h (a), 4 h (b), 8 h (c), 16 h (d), 24 h (e) or 48 h (f). B: OSRGa cells have been treated with 1 µM 12b80 for 1 h (a), 4 h (b), 8 h (c), 16 h (d), 24 h (e) or 48 h (f). Fluorescence of doxorubicin and 12b80 has been evaluated by fluorescence microscopy on living cells. Scale bar = 20 µm.

Range finding of doses of 12b80 in mice. Usable doses of 12b80 in mice were evaluated and compared to doxorubi-

cin (Figure 6). The relationship between dose and toxicity could be verified after single intravenous injection of doxorubicin from 10 to 32.5 µmol/kg, indeed, single doses of 10 or 15 µmol/kg were well tolerated whereas doses of 25 or 32.5 µmol/kg induced severe body weight loss. A correlation between dose and toxicity was also established for 12b80 after single intravenous injection from 32.5 to 100µmol/kg: single doses of 32.5 or 50 µmol/kg were well tolerated whereas doses of 75 µmol/kg or 100 µmol/kg led to severe body weight loss. At the equivalent dose of 32.5 µmol/kg, 12b80 (without any effect on body weight) was not toxic in contrast to doxorubicin treatment, which required euthanasia of animals on D6. As a result, 15 µmol/kg (corresponding to 8.7 mg/kg) was the MTD (maximum tolerated dose) of doxorubicin, in accordance with published data[45,46], while the MTD of 12b80 was set to be 50 µmol/kg. Thus, MTD of 12b80 was more than 3 fold higher than doxorubicin on mice after single injection. Reduction of systemic toxicity of 12b80 compared to doxorubicin could be explained by the specific bone targeting with HBP, and by the prodrug properties with reduction of intracellular intake of complete 12b80. As a result, 12b80 could be used at higher doses than doxorubicin in order to improve its efficacy. Toxicity studies after repeated doses (9 injections) indicated that the maximum usable dose of 12b80 was set at 32.5 µmol/kg (data not shown) whereas is set at 3.4 µmol/kg (corresponding to 2 mg/kg/injection, and 18mg/kg cumulative dose) for doxorubicin[47], which represents around a 10 fold ratio.

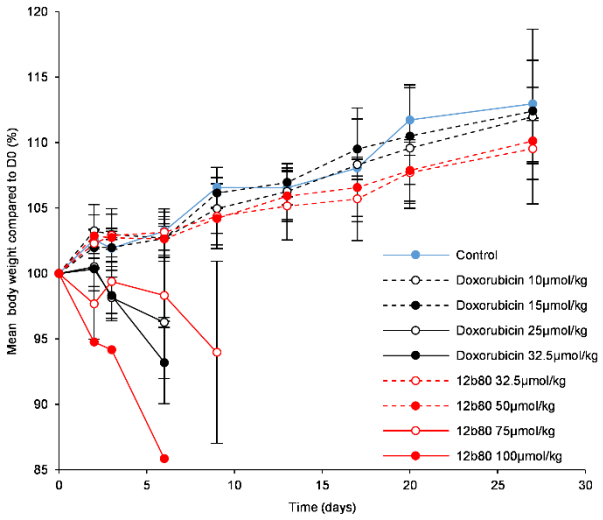

Figure 6: 12b80 prevented systemic toxicity of doxorubicin on body weight. Body weight was monitored following single IV injection of doxorubicin or 12b80 on D0 on Swiss mice (n=3 per group, Mean ± SD).

12b80 distribution in mice. Compound concentration estimated by fluorescence of doxorubicin and derivatives in the tibia was higher after single 12b80 treatment at 32.5 µmol/kg (therapeutic dose) than after doxorubicin treatment at 32.5 µmol/kg (highly toxic dose) at all timepoints from 4 h to 72 h (Figure 7A). The difference was even more noticeable between therapeutic doses of 12b80 (32.5 µmol/kg) and doxorubicin (3.4 µmol/kg). Not only the maximal concentration in bone at first timepoint was higher with 12b80 than with doxorubicin at an equivalent dose, but 12b80 was also more slowly eliminated from the bone tissue. Elimination of fluorescence after 12b80 treatment from the bone was studied for 9 months post-single injection (Figure 7B). Fluorescence intensity in the bone after 3 weeks and 2 months post-treatment represented respectively around 50% and 10% of initial intensity on D1, then remained stable from 2 to 9 months after a single injection. Thus, fluorescent compounds were still detectable in bone 9 months after single 12b80 injection. In the tumor, concentration of fluorescent compounds was much higher after 12b80 treatment at 32.5µmol/kg than after doxorubicin treatment at 3.4 µmol/kg (Figure 7C). At timepoints 24 h and 72 h, fluorescence intensity in tumor was around 10 times higher after 12b80 treatment at 32.5 µmol/kg than after doxorubicin treatment at 3.4 µmol/kg (both at therapeutic dose). In a second step, a histological analysis was carried out on tumor at 24 h post-treatment to demonstrate the distribution of 12b80 on the tumor in comparison with a doxorubicin-treated mouse tumor (Figure 7D). In the tumor, the level of fluorescent compound seemed much higher after 12b80 treatment at 32.5 µmol/kg than after doxorubicin treatment at 3.4 µmol/kg at timepoint 24 h. Furthermore, 12b80 was specifically distributed in mineral nodes inside the tumor (fluorescence area was colocalized with mineralized areas), whereas doxorubicin distribution was more diffuse. Concentration of 12b80 in bone and tumor could not be achieved with doxorubicin. Study with radiolabeled 12b80 over 2 months showed an increasing uptake in bone between 6 and 24 h; thereafter, the activity level remained relatively constant to 72 h and then slowly decreased (Figure 7E). Half-life in bone was around 20 days, and skeleton represented the main target organ on D59. At timepoint 6 h, nearly 10% of injected dose (ID) was distributed in skeleton and was consistent with published data on HBP products[48–50]. All these results demonstrated a rapid distribution of 12b80 in bone tissue in a few hours and a slow elimination within several months. These experiments confirmed the improvement in targeting both bone and bone tumor with doxorubicin when linked to HBP, in terms of concentration and of duration of exposure.

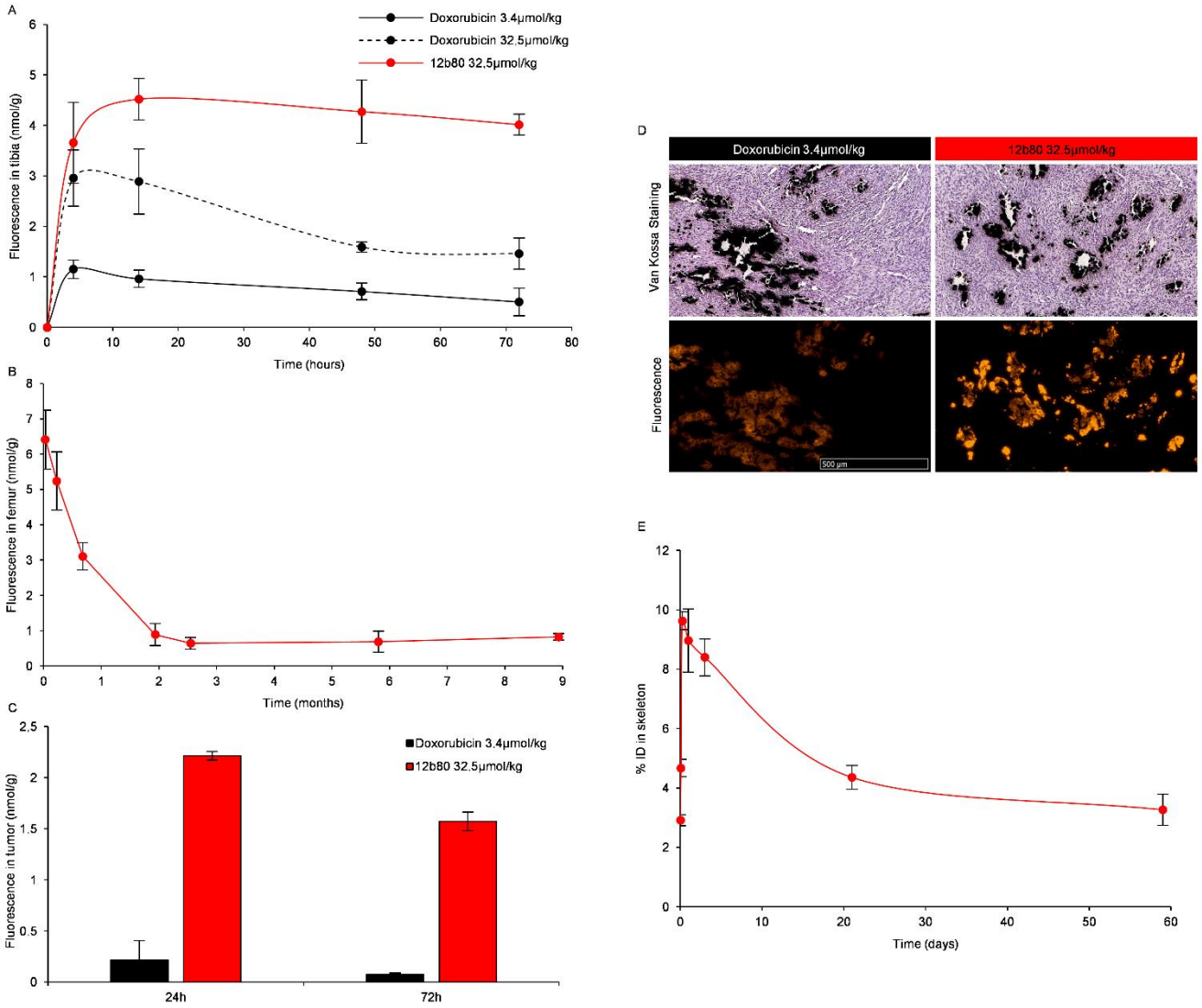

Figure 7: 12b80 distribution in mice. A: 12b80 increased targeting of doxorubicin to bone tissue. Fluorescence* signal was measured by HPLC in the tibia of NMRI Nude mice 4 h to 72 h after single IV injection (Mean ± SD, n=3 per timepoint). B: 12b80 was slowly eliminated from bone. Fluorescence* signal was measured by HPLC in femur of C57BL/6 mice 1 day to 9 months after single IV injection of 12b80 at 32.5 µmol/kg (Mean ± SD, n=3 per timepoint). C: 12b80 increased targeting of doxorubicin to osteosarcoma tumor. Fluorescence* signal was measured by HPLC in orthotopic osteosarcoma tumor (OSRGa) of NMRI Nude mice, 24 or 72 h after single IV injection (Mean ± SD, n=3 per timepoint). D: 12b80 was specifically distributed in mineral nodes inside the tumor. Histological analysis of tumor was carried out on osteosarcoma-bearing NMRI Nude mice (OSRGa) 24 h after single IV treatment with 12b80 at 32.5 µmol/kg or doxorubicin at 3.4 µmol/kg. Slides were stained with Van Kossa and fluorescence was observed at specific channel (fluorescence was excited at 532-554nm and emission was collected at 573-613nm). E: ^{3}H-12b80 distribution in skeleton of mice. Distribution of ^{3}H-12b80 was assessed over 59 days after single IV injection at 32.5 µmol/kg to male Swiss mice (Mean ± SD, n=3 per timepoint). Timepoints: 30 min, 2 h, 6 h, 24 h, 72 h, D21 and D59. Radioactivity was counted in femur and estimated in total skeleton with formula: %ID in skeleton = % ID in femur / 0.02845. (* 3 Fluorescent compounds were detectable by HPLC after bone tissue processing: doxorubicin, doxorubicinone and anthraquinone).

12b80 efficacy in osteosarcoma model in mice. Efficacy of treatment with cycles of repeated injections of 12b80 was evaluated in OSRGa osteosarcoma model. Indeed, this therapeutic scheme every 3 weeks was based on conventional cycle with doxorubicin in human[51]. Anti-tumor efficacy of 12b80 was clearly correlated to injection dose and cumulative dose, with an increase of efficacy from 120 µmol/kg (2x20 µmol/kg x 3 cures) to 293 µmol/kg (3x32.5 µmol/kg x 3 cures) (Figure 8A). Thus, cures of 3 consecutive daily injections every 3 weeks at 32.5 µmol/kg were defined as the best regimen. Efficacy of 12b80 cycles (3x32.5 µmol/kg) was compared to combination of doxorubicin + zoledronate with the same therapeutic scheme (therapeutic doses respectively 3x3.4 and 3x0.34 µmol/kg; i.e. 3x2 mg/kg and 3x100 µg/kg) in the same osteosarcoma model (Figure 8B). 12b80 and doxorubicin were both in-

jected at their maximum tolerated doses. Compared to combination treatment of doxorubicin and zoledronate, 12b80 had a significantly more pronounced antitumor response. On D47, 12b80 treatment reduced tumor volume by 57% compared to doxorubicin/zoledronate combination. 12b80 treatment promoted strong antitumor response highlighted by a reduction of tumor growth and by an inhibition of tumor-associated bone remodeling (reduction of both osteolytic lesions and heterotopic bone formation) (Figure 8C). All together these results demonstrated that maximum efficacy of 12b80 was higher than maximum efficacy of doxorubicin resulting in an increased efficacy/toxicity ratio.

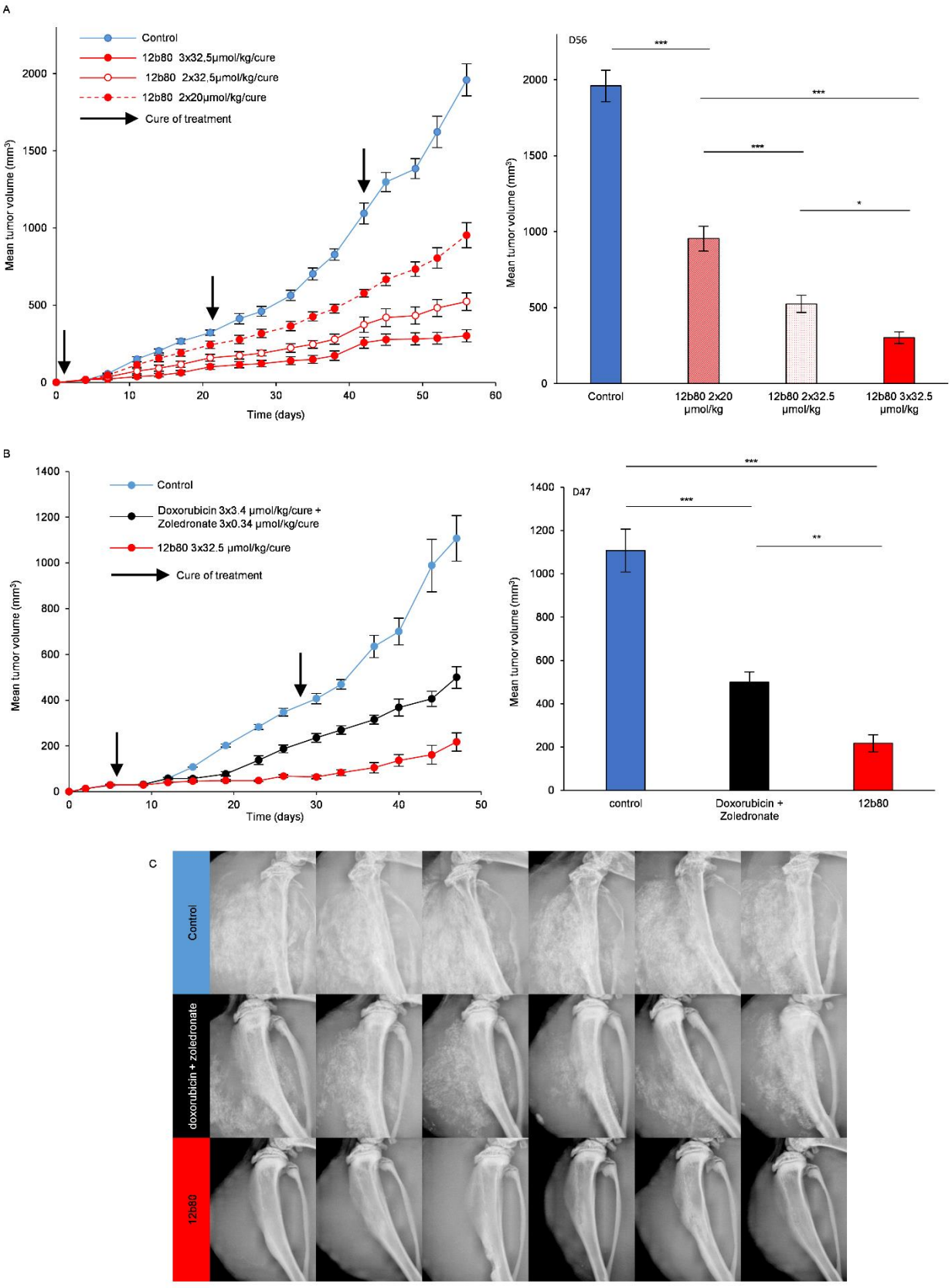

Figure 8: 12b80 efficacy in mice. A: 12b80 treatment reduced tumor growth in osteosarcoma model and displayed a dose-response therapeutic effect. Orthotopic paratibial OSRGa tumors were implanted on D0 in NMRI Nude mice and IV treatment with 12b80 or

DPBS vehicle were administered in cycle every 3 weeks from D1. n=10 mice per group. Mean ± SEM. Statistical analysis at endpoint on D56: Mann Whitney test. * p<0.05, ** p<0.01, *** p<0.001. B: 12b80 was more potent than combination of doxorubicin and zoledronate on osteosarcoma tumor growth. Orthotopic paratibial OSRGa tumors were implanted on D0 in NMRI Nude mice. Mice received IV treatment with DPBS vehicle, 12b80 or doxorubicin+zoledronate every 3 weeks from D6. n=6 mice per group. Mean ± SEM. Statistical analysis on D47: Mann Whitney test. * p<0.05, ** p<0.01, *** p<0.001. C: 12b80 inhibited osteosarcoma-associated bone remodeling. Orthotopic paratibial OSRGa tumors were implanted on D0 in NMRI Nude mice. Mice received IV treatment with DPBS vehicle, 12b80 or doxorubicin+zoledronate every 3 weeks from D6. Radiography of tumor limbs (tibias) was performed on D48 on all mice (n=6 per group).

CONCLUSIONS

The 12b80 molecule consists of three building blocks: the doxorubicin bound by the Linker to the bone targeted HBP Vector through imine bonds. The innovation was based on designed Linker-Vector that played a key role in the acid sensitive doxorubicin release and the high aqueous solubility of the compound. 12b80 displayed rapid and sustained targeting of bone tissue and tumor-associated heterotopic bone and permitted a higher doxorubicin payload in tumor bone environment. Doxorubicin release from 12b80 was dependent on acidic pH associated with active bone tumor environment. 12b80 showed a much lower toxicity compared to doxorubicin. 12b80 promoted strong antitumor effects on rodent orthotopic osteosarcoma, displayed a dose-response therapeutic effect and was more potent than doxorubicin/zoledronate combination. Thus, 12b80 is the first example of cleavable form of HBP-bound doxorubicin with optimized chemical synthesis, detailed physicochemical study, and antitumoral efficacy in preclinical models, that represents a promising new therapy for patients with osteosarcoma, a rare disease with unmet medical needs. Therapeutic indications of 12b80 could presumably be extended to other kinds of tumors that develop in bone environment, such as Ewing sarcoma, myeloma, but also in bone metastases secondary to breast or prostate cancer and could benefit to substantially more patients.

EXPERIMENTAL PROCEDURES

Synthesis. The methods of synthesis of compounds **2 - 5** are available in the Supporting Information.

Vector. The dry acid **5** (30 g, 97 mmol, 1 eq) was solubilized in dry THF (150 mL, water bath 55°C) under argon using magnetic stirring. Triethylamine (13.5 mL, 97 mmol, 1 eq) was added and the reaction medium was cooled down to 10 °C by using an ice bath. Pivaloyl chloride (11.8 mL, 97 mmol, 1 eq) was added dropwise and the reaction medium was stirred for 20 min under ice bath cooling. The reaction medium was filtered under argon to remove triethylamine salt, the $P(OSiMe_3)_3$ (97.2 mL, 291 mmol, 3 eq) was quickly added and the reaction medium was stirred for 1 h at room temperature under argon. Methanol (100 mL) was added and the reaction medium was stirred for 10-15 min. Ether (500 mL) was added, the precipitate was separated and washed 3 times with ether (50 mL). The product was dried under vacuum and solubilized in water (25 mL) and after 15 min 12N NaOH (around 16 mL, 1 eq) was added until reaching pH=7. Methanol was added (250 mL) and precipitate was obtained by addition of ether (400 mL). The solid was filtered off, washed with ether and dried under vacuum at room temperature. The **Vector** was obtained as a white powder (32.2 g, purity 82% by ^{1}H NMR, 60% yield). HRMS: $[M - H]^-$ m/z = 410.0779; calc. for $C_{14}H_{22}NO_9P_2$ = 410.0775. ^{1}H NMR (D_2O, 400 MHz): δ 9.74 (s, 1H), 7.41 (m, 3H), 7.21 (d, 1H), 4.09 (t, 2H), 3.29 (br m, 4H), 2.76 (s, 3H), 2.21 (br m, 2H), 2.13 (br m, 2H). ^{31}P NMR (D_2O, 162 MHz): δ 17.25.

Linker. Thiocarbohydrazide (66 g, 630 mmol, 4 eq) was solubilized in DMSO (400 mL) at 85 °C under argon using magnetic stirring. After solubilization the solution was cooled to room temperature without stirring. Compound **6** (40 g, 120 mmol, 1 eq) was solubilized in DMSO (216 mL) at 85 °C under argon using magnetic stirring. The hot solution of compound **6** was added by syringe to the solution of thiocarbohydrazide at room temperature in 10 min using vigorous stirring (1000 rpm). Reaction mixture was stirred for 45 min and then diluted with ethylene glycol (200 mL). Then acetonitrile was added (2.4 L) using vigorous stirring (1000 rpm), which resulted in the precipitation of the **Linker**. The mixture was stirred for 15 min. The precipitate was filtered off and washed twice with a mixture of ethylene glycol/MeCN=1/3 (100 mL) and then 4 times with MeCN (100 mL). The solid was dried under vacuum on rotavapor at 30 °C. The residual solid was solubilized in ethylene glycol (240 mL) at 40 °C. MeCN (720 mL) was gradually added to the brown solution obtained using vigorous stirring (1000 rpm) to precipitate the **Linker**. The mixture was stirred for 15 min at room temperature. The precipitate was filtered off and washed 3 times with a mixture of ethylene glycol/MeCN=1/3 (100 mL) and then 3 times with MeCN (100 mL). The solid was transferred to a round bottom flask, MeCN (200 mL) was added and the mixture was stirred for 15 min at room temperature. The off-white **Linker** (45 g, 80 % yield) was filtered off, washed twice with MeCN (100 mL) and dried under vacuum on rotavapor at 30 °C. HRMS: $[M - H]^-$ m/z = 467.1247; calc. for $C_{12}H_{23}N_{10}O_6S_2$ = 467.1249. ^{1}H NMR (D2O, 400 MHz): δ 3.87 (2H, s), 3.70 (2H, s), 3.24 (2H, s).

Linker-Vector. The solution of the **Vector** (1.7 g, 3.7 mmol, 1 eq) and TFA (1 mL) in DMSO (23 mL) was added dropwise (3 min) to the solution of the **Linker** (4.5 g, 9.6 mmol, 2.5 eq) in DMSO (12 mL) at room temperature under vigorous stirring. The reaction mixture was stirred 5 min at room temperature then diluted with THF (175 mL), stirred 15 min. The precipitate was filtered off, washed with THF, dried under vacuum at 30 °C and solubilized in DMSO (23 mL) at 40 °C. Under the vigorous stirring the THF (60 mL) was added. After 15 min the precipitate was filtered off, washed with THF, and dried under vacuum at 30 °C. The **Linker-Vector** was obtained (2.6 g, 80% yield) as a white powder. HRMS: $[M - H]^-$ m/z = 860.2009; calc.

for $C_{26}H_{44}N_{11}O_{14}P_2S_2$ = 860.1991. ^{1}H NMR (D_2O, 400 MHz): δ 8.15-6.85 (5H, m), 4.25-2.95 (18H, m), 2.87 (3H, s), 2.34 (2H, m), 2.23 (2H, m). ^{31}P NMR (D_2O, 162 MHz): δ 17.73.

12b80. **Doxorubicin** hydrochloride (500 mg, 0.86 mmol, 1 eq) and the **Linker-Vector** (1600 mg, 1.85 mmol, 2.2 eq) were mixed under argon in the solution of 1% TFA/DMSO (20 mL). The solution was stirred 4 h at room temperature under argon. The THF (80 mL) was added, the reaction mixture was stirred 15 min and then the precipitate was filtered, washed with THF and dried under vacuum at 30°C. Crude **12b80** was obtained as a red solid (1.8 g) and solubilized in 0.5M $NaHCO_3$ (15 mL). The solution was injected with a syringe in the C18 column (220 g) and eluted in the gradient from 3% EtOH to 15% EtOH. Fractions with a purity >90% (HPLC control) were mixed, concentrated under vacuum at 30 °C and lyophilized. **12b80** was obtained as a sodium salt (450 mg, 36% yield, HPLC: 95%). HRMS: $[M + H]^+$ m/z = 1387.3812; calc. for $C_{53}H_{73}N_{12}O_{24}P_2S_2$ = 1387.3772. ^{1}H NMR (1%TFA-D/DMSO-D_6, 400 MHz): δ 14.07 (1H, s), 13.36 (1H, s), 11.97 (1H, s), 11.24 (1H, s), 10.53 (1H, s), 10.48 (1H, s), 10.30 (1H, s), 9.80 (1H, s), 8.05 (1H, s), 7.95 (2H, s), 7.84 (2H, m), 7.68 (1H, dd), 7.46 (1H, s), 7.40 (1H, d), 7.33 (1H, t), 7.02 (1H, d), 5.30 (1H, s), 4.99 (1H, s), 4.61 (1H, t), 4.5-3.7 (12H, m), 3.6-2.85 (14H, m), 3.01 (1H, d), 2.81 (3H, s), 2.27 (4H, m), 2.13 (2H, m), 1.85 (1H, t), 1.65 (1H, d), 1.18 (3H, d). ^{31}P NMR (1%TFA-D/DMSO-D_6, 162 MHz): δ 18.23.

Safety. As for cytotoxic agents, doxorubicin and 12b80 were handled with care using gloves, masks, lab coats and glasses for solutions, and under chemical fume hood in addition for powder.

Physicochemical characterization. Flash chromatography purification was conducted using a Gilson PLC2020 system using C18 cartridges from Macherey Nagel. Thin layer chromatography (TLC) was performed on Merck Silica Gel 60 F254 plates, and the developed plates were visualized under a UV lamp at 254 nm. NMR spectra were recorded at 400 MHz for ^{1}H and 163 MHz for ^{31}P at 303 K on samples dissolved in the appropriate deuterated solvent. Used references were the deuterated solvent signal for residual ^{1}H. Chemical displacement values (δ) are expressed in parts per million (ppm) and coupling constants (J) in hertz (Hz). HRMS analyses were carried out on Orbitrap mass spectrometer (ESI). HPLC studies were conducted using Waters system with a Phenomenex Luna Column 5u C18(2) 100Å 150x4.6 mm. Chromatographic conditions were as follows: flow 1.0 ml/min; mobile phase A - ammonium acetate 20 mM and 0,02% $EDTANa_2$ and NH_4OH (pH=8.7), B - acetonitrile, injection volume 20 µL; gradient, initial mobile phase 5% B, 0-10 min increased to 70%, 10-12 min 70%B, 12-14 min decreased to initial mobile phase. Fluorescence detection was performed at 480 nm for excitation and 558 nm for emission (2475 FLR detector Waters), UV detection was performed at 275 nm. All reagents were purchased from Sigma-Aldrich or TCI and were used as supplied by the manufacturer.

Binding assay. Hydroxyapatite was purchased from Biorad. Bovine bone (femur) was crushed after freezing in liquid nitrogen. 50 mg of tissue or HA were suspended in a 12b80 solution (1.4 mM; 5 mL). The mixture was stirred 30 min at room temperature (360° rotation stirrer). After centrifugation, the supernatant was removed and analyzed by HPLC-UV to determine the concentration and then to calculate the rate of binding.

Drug release studies. 90 mg of HA were suspended in a 12b80 solution (1.1 mM; 6 mL) and stirred 30 min at room temperature (360° rotation stirrer). HA-bound 12b80 was washed with 0.9% NaCl (3x3 mL), filtered and washed with methanol, and dried under vacuum. 5 mg of 12b80-HA was suspended in 500 µL of solution in Eppendorf tube at 37 °C in an oven. 4 solutions were used: DPBS (pH 7.4) or citrate buffer (pH 6, 5, 4). All the solvent was removed at 24 h, 48 h and 72 h, diluted (1/2) with 7 mM EDTA and analyzed by HPLC. 500 µL of solution was added to the residual 12b80-HA between each timepoint.

Cell line. Rat OSRGa cell line was established from an initially radio-induced osteosarcoma[52]. OSRGa cells were grown in DMEM cell culture medium supplemented with 10% fetal bovine serum in a humidified 5% CO_2 chamber at 37 °C. Mouse fibroblast L929 cells were grown in RPMI cell culture medium supplemented with 10% fetal bovine serum in a humidified 5% CO_2 chamber at 37 °C.

Cell viability assay. Cell viability was quantified by measuring metabolic activity with WST-1 assay (Roche). Briefly, OSRGa cells were plated into 96-Well-Plates at an initial density of 2000 cells/well and L929 cells were plated at an initial density of 1000 cells/well. Cells were grown in a humidified 5% CO_2 chamber at 37 °C in their respective cell culture media. After 24 h, cells were treated for 72 h with doxorubicin (dissolved in water) or with 12b80 (dissolved in DPBS) at concentrations ranging from 5 nM to 50 µM, or with their respective control solvent. Cell viability was evaluated after 72h by measuring the reduction of tetrazolium salt WST-1 to formazan at 37 °C. Absorbance of the reduction reaction was read at 420 and 480 nm. Measure was stopped when the absorbance of solvent treated cells reached a value between 1.5 and 2. Each condition was performed in triplicate wells.

In-vitro comparison of doxorubicin and 12b80 cellular drug uptake and distribution. OSRGa cells were plated on glass coverslip into 12 wells plate at a concentration of 25000 cells/well. Cells were incubated in a humidified 5% CO_2 chamber at 37 °C. After 96 h, cells were treated with 1 µM of 12b80 or doxorubicin for 1, 4, 8, 16, 24 or 48 h at 37 °C. Fluorescence images were obtained with a Nikon Eclipse 80i microscope on living cells at a 400x magnification. Doxorubicin-associated fluorescence was excited at 532-554 nm and emission was collected at 573-613 nm.

Animals. All procedures and experimental protocols used in this study were in compliance with the 2010/63/EU directive of the European Parliament, for the protection of

animals used for scientific purposes. All experiments were approved by French Research Ministry (project authorization APAFIS#2193 and MESR#01489-01) and were in accordance with the institutional guidelines of the Regional Ethical Committee for animal experiment (CEEA PdL06). Mice were purchased from Janvier Labs and were acclimatized for a minimum of 7 days prior to the beginning of the study. 5 to 6 week old male Swiss mice, male and female C57BL/6 mice, and female NMRI Nude mice were included in protocols. All animals were housed in pathogen-free and controlled conditions (temperature 22±2 °C, humidity 55±10%) on a 12 h light-dark cycle, in cages of 3 to 5 animals. All animals had free access to 0.2 µm filtered water and were fed ad libitum with a commercial chow. Animals were identified by individual ear tags, randomly distributed in 3 to 10 animals per group and monitored every day for clinical status. As a general measure of gross toxicity, body weight monitoring was performed twice a week. Euthanasia was performed by cervical dislocation under isoflurane inhalation anesthesia.

Experimental osteosarcoma model. Osteosarcoma model was induced by injection of OSRGa rat osteosarcoma cell line to NMRI nude mice. $2x10^6$ cells in 15 µL of DPBS were injected in close contact with the right tibia, after light periost scratching, on mice anesthetized by isoflurane inhalation (air 0.5 L/min and isoflurane 2%). Tumor volume was quantified twice a week by measuring two perpendicular diameters with a Vernier caliper and calculated with the formula: $(l^2 \times L)/2$ (l, the smallest and L, the largest diameter). Mice with tumor volumes exceeding 2500 mm^3 were sacrificed. Radiography of the right tibia was performed on each animal using a radiography unit (Faxitron) after euthanasia.

Treatment of rodents. 12b80 powder was solubilized in DPBS. Doxorubicin powder was purchased from AOKchem and solubilized in 0.9% NaCl. Zoledronate was purchased from TCI and solubilized in DPBS. Mice were treated with intravenous bolus injection of 12b80 or doxorubicin at 10 mL/kg in tail vein using 29G insulin syringe. Zoledronate was administered by subcutaneous injection at 1 mL/kg. For MTD evaluation, Swiss mice were treated on D0 by single injection of doxorubicin (10 to 32.5 µmol/kg) or 12b80 (32.5 to 100 µmol/kg) and euthanized on D27. For analysis of distribution in healthy femurs, C57BL/6 mice were treated on D0 by single injection of 12b80 (32.5 µmol/kg) and sacrificed between 1 day and 9 months post-injection. For analysis of distribution in tumors and healthy tibias, OSRGa tumors were inoculated on NMRI nude mice on D0, mice received single injection of doxorubicin (3.4 or 32.5 µmol/kg) or 12b80 (32.5 µmol/kg) on D33 and were euthanized 4 h to 72 h post-injection. For dose-response efficacy study, OSRGa tumors were inoculated on NMRI nude mice on D0, mice were treated with 12b80 (20 or 32.5 µmol/kg) from D1 on 2 or 3 consecutive days every 3 weeks and were sacrificed between D53 and D66 according to tumor volume. For antitumor efficacy comparison to reference treatment, OSRGa tumors were inoculated on NMRI Nude mice on D0, mice received injection of 12b80 (32.5 µmol/kg) or doxorubicin (3.4 µmol/kg) associated with zoledronate (0.34 µmol/kg) from D6 on 3 consecutive days every 3 weeks and were euthanized on D48.

Histological analysis. For analysis of distribution in tumor, tissues were sampled 24 h post-injection, fixed in 4% formalin, dehydrated in 70% ethanol and with automatized system (Leica), embedded in paraffin and stored at 4 °C. Each sample was sectioned using a microtome (Microm Microtech). 4-µm-thick sections were cut and affixed on treated histological slides (Super frost plus – Thermo scientific). Fluorescence was observed on sections in a specific channel (fluorescence was excited at 532-554 nm and emission was collected at 573-613 nm) to localize 12b80- and/or metabolites-associated fluorescence. Sections were then stained with Van Kossa to localize tumor mineral nodes. Nanozoomer (Hamamatsu) was used for images acquisition.

HPLC analysis of biodistribution. For analysis of distribution in tibia, femur and tumor, samples were collected, stored at -20 °C and crushed in liquid nitrogen with a mortar. A weighed quantity of tissue (50 to 200 mg) was dispersed in 6N HCl (0.75 mL) stirred at ambiant temperature for 18 h. The mixture was extracted with a solution of $CHCl_3$ and MeOH (9/1; 0.75 mL). The organic layer was collected and the volatiles were removed under air flow. The residue was solubilized in CH_3CN (200 µL), centrifuged and analysed by HPLC (waters system). Total fluorescence was presented in nmol/g of tissue as sum of concentration of main products in samples: doxorubicin, doxorubicinone and anthraquinone.

Radiolabelling. ^{3}H-12b80 was synthesized starting from ^{3}H-doxorubicin (Moravek) using the same strategy described in Figure 1. ^{3}H-12b80 was administered intravenously at 32.5 µmol/kg to male Swiss mice. The distribution of ^{3}H-12b80 in bones was assessed over 59 days. 3 mice were sacrificed at each timepoint and femurs were collected, rinsed with 0.9% NaCl, blot-dried and weighed using a precision scale and put into scintillation vial. 1 mL of 6N HCl was added in each sample and vial was stirred at room temperature for 72 to 96 h. Then, 1.5 mL of solubilizing solution (Solvable™ Tissue Solubilizer - Perkin Elmer) was added and vials were placed overnight at 56 °C. The discoloration was performed by addition of 0.3 mL 30% hydrogen peroxide. 10 mL of liquid scintillation cocktail (LLT Ultima Gold - Perkin Elmer) was then added and vials were placed in darkness before counting to allow decay of luminescence. Then, tubes were placed under an automatic TDCR liquid scintillation counter (Hidex 300 SL) calibrated for tritium radionuclide. 40 seconds per sample was needed to count the radioactivity. Radioactivity was given in disintegrations per minute (dpm). The radioactivity in bone samples was expressed as percentage of the injected dose (ID) per gram of bone. % of ID in total skeleton was estimated with following formula: %ID skeleton = % ID femur / 0.02845. This formula was based on the analysis of weight of femur vs weight of total skeleton in mice from

the same strain and same age. In this study of 4 week old mice, femurs represented 2.845% of total skeleton weight.

Statistical methods. *In-vitro* studies of binding, drug release and cell viability were performed in triplicate and presented as Mean ± SD. *In-vivo* studies of MTD or distribution were conducted on 3 animals per group and timepoint; body weight or total fluorescence were presented in Mean ± SD, but no statistical analysis was performed on these small samples. *In-vivo* studies of efficacy were conducted on 10 mice per group (dose-response efficacy study) or 6 mice per group (efficacy comparison to reference treatment) and tumor volumes were presented as Mean ± SEM. Statistical analysis was presented for the last measurement of tumor volume, by Mann Whitney test. Statistical analysis was performed using Prism3 and excel softwares. Probability values of less than 0.05 (two-tailed) were used as the critical level of significance for all tests. Mean values were annotated with an asterisk symbol (* p-value < 0.05, ** p-value < 0.01 and *** p-value < 0.001).

ASSOCIATED CONTENT

Supporting Information. General methods and instrumentation; NMR and HRMS spectra. This material is available free of charge via the Internet at http://pubs.acs.org

AUTHOR INFORMATION

Corresponding Author

* Emmanuelle David. Atlanthera, 3 rue Aronnax, 44821 Saint Herblain, France. emmanuelle.david@atlanthera.com

Author Contributions

R. Le Bot conceived the project. M. Egorov designed the synthetic and purification work which was carried out by J.Y. Goujon, L. Morandeau and M. Egorov. J.Y. Goujon developed the analytical and bioanalytical methods which were carried out by M. Egorov, L. Morandeau and J.Y. Goujon. S. Cagnol designed the *in-vitro* biological studies, which were conducted by J. Taurelle, M. Sicard and S. Cagnol. E. David monitored the project planning and designed the *in-vivo* biological studies, which were carried out by J. Taurelle, C. Moal, M. Sicard, C. Benesteau, S. Pairel and E. David. E. David wrote this paper, with the contribution of S. Cagnol, J.Y. Goujon and M. Egorov. D. Heymann, F. Redini and F. Gouin were part of the scientific committee for the project. All authors have given approval to the final version of the manuscript.

ACKNOWLEDGMENT

Rat osteosarcoma OSRGa has been kindly given by Pr F Redini from INSERM UMR1238 unit, Nantes, France. Radiolabelling synthesis and studies was performed by Chelatec, Saint Herblain, France.

ABBREVIATIONS

BP: bisphosphonate; D: day; DPBS: Dulbecco's Phosphate-Buffered Saline; EFS: event-free survival; HA: hydroxyapatite; HBP: hydroxybisphosphonate; IC50 : half maximal inhibitory concentration; ID: injected dose; MTD: maximum tolerated dose.

REFERENCES

(1) Mirabello, L.; Troisi, R. J.; Savage, S. A. Osteosarcoma Incidence and Survival Rates from 1973 to 2004: Data from the Surveillance, Epidemiology, and End Results Program. Cancer 2009, 115 (7), 1531–1543. https://doi.org/10.1002/cncr.24121.

(2) American Cancer Society. Key Statistics for Osteosarcoma. January 24, 2018.

(3) Valery, P. C.; Laversanne, M.; Bray, F. Bone Cancer Incidence by Morphological Subtype: A Global Assessment. Cancer Causes Control 2015, 26 (8), 1127–1139. https://doi.org/10.1007/s10552-015-0607-3.

(4) Isakoff, M. S.; Bielack, S. S.; Meltzer, P.; Gorlick, R. Osteosarcoma: Current Treatment and a Collaborative Pathway to Success. J Clin Oncol 2015, 33 (27), 3029–3035. https://doi.org/10.1200/JCO.2014.59.4895.

(5) Ferrari, S.; Serra, M. An Update on Chemotherapy for Osteosarcoma. Expert Opinion on Pharmacotherapy 2015, 16 (18), 2727–2736. https://doi.org/10.1517/14656566.2015.1102226.

(6) Anninga, J. K.; Gelderblom, H.; Fiocco, M.; Kroep, J. R.; Taminiau, A. H. M.; Hogendoorn, P. C. W.; Egeler, R. M. Chemotherapeutic Adjuvant Treatment for Osteosarcoma: Where Do We Stand? Eur. J. Cancer 2011, 47 (16), 2431–2445. https://doi.org/10.1016/j.ejca.2011.05.030.

(7) Bacci, G.; Briccoli, A.; Rocca, M.; Ferrari, S.; Donati, D.; Longhi, A.; Bertoni, F.; Bacchini, P.; Giacomini, S.; Forni, C.; et al. Neoadjuvant Chemotherapy for Osteosarcoma of the Extremities with Metastases at Presentation: Recent Experience at the Rizzoli Institute in 57 Patients Treated with Cisplatin, Doxorubicin, and a High Dose of Methotrexate and Ifosfamide. Ann. Oncol. 2003, 14 (7), 1126–1134.

(8) Kim, W.; Han, I.; Lee, J. S.; Cho, H. S.; Park, J. W.; Kim, H.-S. Postmetastasis Survival in High-Grade Extremity Osteosarcoma: A Retrospective Analysis of Prognostic Factors in 126 Patients. J Surg Oncol 2018, 117 (6), 1223–1231. https://doi.org/10.1002/jso.24963.

(9) Wu, J.; Sun, H.; Li, J.; Guo, Y.; Zhang, K.; Lang, C.; Zou, C.; Ma, H. Increased Survival of Patients Aged 0-29 Years with Osteosarcoma: A Period Analysis, 1984-2013. Cancer Med 2018, 7 (8), 3652–3661. https://doi.org/10.1002/cam4.1659.

(10) Puljula, E.; Turhanen, P.; Vepsäläinen, J.; Monteil, M.; Lecouvey, M.; Weisell, J. Structural Requirements for Bisphosphonate Binding on Hydroxyapatite: NMR Study of Bisphosphonate Partial Esters. ACS Med Chem Lett 2015, 6 (4), 397–401. https://doi.org/10.1021/ml5004603.

(11) Cole, L. E.; Vargo-Gogola, T.; Roeder, R. K. Targeted Delivery to Bone and Mineral Deposits Using Bisphosphonate Ligands. Advanced Drug Delivery Reviews 2016, 99, 12–27. https://doi.org/10.1016/j.addr.2015.10.005.

(12) Van Poznak, C. H.; Temin, S.; Yee, G. C.; Janjan, N. A.; Barlow, W. E.; Biermann, J. S.; Bosserman, L. D.; Geoghegan, C.; Hillner, B. E.; Theriault, R. L.; et al. American

Society of Clinical Oncology Executive Summary of the Clinical Practice Guideline Update on the Role of Bone-Modifying Agents in Metastatic Breast Cancer. JCO 2011, 29 (9), 1221–1227. https://doi.org/10.1200/JCO.2010.32.5209.

(13) Yusuf, A. A.; Cummings, S. R.; Watts, N. B.; Feudjo, M. T.; Sprafka, J. M.; Zhou, J.; Guo, H.; Balasubramanian, A.; Cooper, C. Real-World Effectiveness of Osteoporosis Therapies for Fracture Reduction in Post-Menopausal Women. Arch Osteoporos 2018, 13 (1), 33. https://doi.org/10.1007/s11657-018-0439-3.

(14) Abdelkarim, M.; Guenin, E.; Sainte-Catherine, O.; Vintonenko, N.; Peyri, N.; Perret, G. Y.; Crepin, M.; Khatib, A.-M.; Lecouvey, M.; Di Benedetto, M. New Symmetrically Esterified M-Bromobenzyl Non-Aminobisphosphonates Inhibited Breast Cancer Growth and Metastases. PLoS One 2009, 4 (3). https://doi.org/10.1371/journal.pone.0004685.

(15) Guenin, E.; Ledoux, D.; Oudar, O.; Lecouvey, M.; Kraemer, M. Structure-Activity Relationships of a New Class of Aromatic Bisphosphonates That Inhibit Tumor Cell Proliferation In Vitro. Anticancer Res 2005, 25 (2A), 1139–1145.

(16) Fleisch, H.; Russell, R. G.; Bisaz, S.; Casey, P. A.; Mühlbauer, R. C. The Influence of Pyrophosphate Analogues (Diphosphonates) on the Precipitation and Dissolution. Calcif Tissue Res 1968, Suppl:10-10a.

(17) Beek, E. van; Hoekstra, M.; Ruit, M. van D.; Löwik, C.; Papapoulos, S. Structural Requirements for Bisphosphonate Actions in Vitro. Journal of Bone and Mineral Research 1994, 9 (12), 1875–1882. https://doi.org/10.1002/jbmr.5650091206.

(18) Beek, E. van; Löwik, C.; Que, I.; Papapoulos, S. Dissociation of Binding and Antiresorptive Properties of Hydroxybisphosphonates by Substitution of the Hydroxyl with an Amino Group. Journal of Bone and Mineral Research 1996, 11 (10), 1492–1497. https://doi.org/10.1002/jbmr.5650111016.

(19) Egorov, M.; Fortun, Y.; Heymann, D.; Lebreton, J.; Mathe, M.; Padrines, M.; Redini, F. Method for Synthesizing Hydroxy-Bisphosphonic Acid Derivatives. PCT Int. Appl. (2009), WO 2009083613 A1 20090709.

(20) Hu, R.; Zheng, H.; Cao, J.; Davoudi, Z.; Wang, Q. Synthesis and In Vitro Characterization of Carboxymethyl Chitosan-CBA-Doxorubicin Conjugate Nanoparticles as pH-Sensitive Drug Delivery Systems https://www.ingentaconnect.com/content/asp/jbn/2017/00000013/00000009/art00008 (accessed Apr 23, 2019). https://doi.org/info:doi/10.1166/jbn.2017.2407.

(21) Hu, R.; Zheng, H.; Cao, J.; Davoudi, Z.; Wang, Q. Self-Assembled Hyaluronic Acid Nanoparticles for pH-Sensitive Release of Doxorubicin: Synthesis and In Vitro Characterization https://www.ingentaconnect.com/content/asp/jbn/2017/00000013/00000009/art00004 (accessed Apr 23, 2019). https://doi.org/info:doi/10.1166/jbn.2017.2406.

(22) Zhang, X.; Zhang, H.; Yin, L.; Hu, R.; Qiu, T.; Yin, Y.; Xiong, X.; Zheng, H.; Wang, Q. A PH-Sensitive Nanosystem Based on Carboxymethyl Chitosan for Tumor-Targeted Delivery of Daunorubicin. J Biomed Nanotechnol 2016, 12 (8), 1688–1698.

(23) Zheng, H.; Yin, L.; Zhang, X.; Zhang, H.; Hu, R.; Yin, Y.; Qiu, T.; Xiong, X.; Wang, Q. Redox Sensitive Shell and Core Crosslinked Hyaluronic Acid Nanocarriers for Tumor-Targeted Drug Delivery. J Biomed Nanotechnol 2016, 12 (8), 1641–1653.

(24) Rudnick-Glick, S.; Corem-Salkmon, E.; Grinberg, I.; Yehuda, R.; Margel, S. Near IR Fluorescent Conjugated Poly(Ethylene Glycol)Bisphosphonate Nanoparticles for in Vivo Bone Targeting in a Young Mouse Model. J Nanobiotechnology 2015, 13. https://doi.org/10.1186/s12951-015-0126-0.

(25) Rudnick-Glick, S.; Corem-Salkmon, E.; Grinberg, I.; Margel, S. Targeted Drug Delivery of near IR Fluorescent Doxorubicin-Conjugated Poly(Ethylene Glycol) Bisphosphonate Nanoparticles for Diagnosis and Therapy of Primary and Metastatic Bone Cancer in a Mouse Model. J Nanobiotechnology 2016, 14. https://doi.org/10.1186/s12951-016-0233-6.

(26) Farrell, K. B.; Karpeisky, A.; Thamm, D. H.; Zinnen, S. Bisphosphonate Conjugation for Bone Specific Drug Targeting. Bone Rep 2018, 9, 47–60. https://doi.org/10.1016/j.bonr.2018.06.007.

(27) Young, R. N.; Grynpas, M. D. Targeting Therapeutics to Bone by Conjugation with Bisphosphonates. Current Opinion in Pharmacology 2018, 40, 87–94. https://doi.org/10.1016/j.coph.2018.03.010.

(28) Morton, S. W.; Shah, N. J.; Quadir, M. A.; Deng, Z. J.; Poon, Z.; Hammond, P. T. Osteotropic Therapy via Targeted Layer-by-Layer Nanoparticles. Adv Healthc Mater 2014, 3 (6), 867–875. https://doi.org/10.1002/adhm.201300465.

(29) Zinnen, S. P.; Karpeisky, A.; Hoff, D. D. V.; Plekhova, L.; Alexandrov, A. First-in-Human Phase I Study of MBC-11, a Novel Bone-Targeted Cytarabine-Etidronate Conjugate in Patients with Cancer-Induced Bone Disease. The Oncologist 2018, theoncologist.2018-0707. https://doi.org/10.1634/theoncologist.2018-0707.

(30) Ye, W.-L.; Zhao, Y.-P.; Na, R.; Li, F.; Mei, Q.-B.; Zhao, M.-G.; Zhou, S.-Y. Actively Targeted Delivery of Doxorubicin to Bone Metastases by a PH-Sensitive Conjugation. JPharmSci 2015, 104 (7), 2293–2303. https://doi.org/10.1002/jps.24476.

(31) Hochdörffer, K.; Abu Ajaj, K.; Schäfer-Obodozie, C.; Kratz, F. Development of Novel Bisphosphonate Prodrugs of Doxorubicin for Targeting Bone Metastases That Are Cleaved PH Dependently or by Cathepsin B: Synthesis, Cleavage Properties, and Binding Properties to Hydroxyapatite As Well As Bone Matrix. J. Med. Chem. 2012, 55 (17), 7502–7515. https://doi.org/10.1021/jm300493m.

(32) Kratz, F. Bisphosphonate-Prodrugs. WO2011023367A3.

(33) Egorov, M.; Goujon, J.-Y.; Le Bot, R.; David, E. Hydrosoluble Hydroxy-Bisphosphonic Derivatives of Doxorubicin. PCT Int. Appl. (2016), WO 2016079327 A1.

(34) Egorov, M.; Goujon, J.-Y.; Le Bot, R. Bifunctional Hydroxy-Bisphosphonic Acid Derivatives. PCT Int. Appl. (2012), WO 2012130911 A1 20121004.

(35) Egorov, M.; Fortun, Y.; Heymann, D.; Lebreton, J.; Mathe, M.; Padrines, M.; Redini, F. Hydroxy-Bisphosphonic Acid Derivatives as Vectors for Therapeutic and Diagnostic Targeting of Bone Tissue. PCT Int. Appl. (2009), WO 2009083614 A1 2009070.

(36) Egorov, M.; Aoun, S.; Padrines, M.; Redini, F.; Heymann, D.; Lebreton, J.; Mathe, M. A One-Pot Synthesis of 1-Hydroxy-1,1-Bis(Phosphonic Acid)s Starting from the Corresponding Carboxylic Acids. Eur. J. Org. Chem 2011, 7148–7154.

(37) Lecouvey, M. A Mild and Efficient One-Pot Synthesis of 1-Hydroxymethylene-1,1-Bisphosphonic Acids. Preparation of New Tripod Ligands. Tetrahedron Letters.

(38) Anderson, M.; Moshnikova, A.; Engelman, D. M.; Reshetnyak, Y. K.; Andreev, O. A. Probe for the Measurement of Cell Surface PH in Vivo and Ex Vivo. Proc Natl Acad Sci U S A 2016, 113 (29), 8177–8181. https://doi.org/10.1073/pnas.1608247113.

(39) Vaupel, P.; Kallinowski, F.; Okunieff, P. Blood Flow, Oxygen and Nutrient Supply, and Metabolic Microenvironment of Human Tumors: A Review. Cancer Res 1989, 49 (23), 6449–6465.

(40) Silver, I. A.; Murrills, R. J.; Etherington, D. J. Microelectrode Studies on the Acid Microenvironment beneath Adherent Macrophages and Osteoclasts. Exp. Cell Res. 1988, 175 (2), 266–276.

(41) Susa, M.; Iyer, A. K.; Ryu, K.; Hornicek, F. J.; Mankin, H.; Amiji, M. M.; Duan, Z. Doxorubicin Loaded Polymeric Nanoparticulate Delivery System to Overcome Drug Resistance in Osteosarcoma. BMC Cancer 2009, 9, 399. https://doi.org/10.1186/1471-2407-9-399.

(42) Coxon, F. P.; Thompson, K.; Roelofs, A. J.; Ebetino, F. H.; Rogers, M. J. Visualizing Mineral Binding and Uptake of Bisphosphonate by Osteoclasts and Non-Resorbing Cells. Bone 2008, 42 (5), 848–860. https://doi.org/10.1016/j.bone.2007.12.225.

(43) Verhulst, A.; Sun, S.; McKenna, C. E.; D'Haese, P. C. Endocytotic Uptake of Zoledronic Acid by Tubular Cells May Explain Its Renal Effects in Cancer Patients Receiving High Doses of the Compound. PLoS One 2015, 10 (3). https://doi.org/10.1371/journal.pone.0121861.

(44) Thompson, K.; Rogers, M. J.; Coxon, F. P.; Crockett, J. C. Cytosolic Entry of Bisphosphonate Drugs Requires Acidification of Vesicles after Fluid-Phase Endocytosis. Mol. Pharmacol. 2006, 69 (5), 1624–1632. https://doi.org/10.1124/mol.105.020776.

(45) Bertazzoli, C.; Rovero, C.; Ballerini, L.; Lux, B.; Balconi, F.; Antongiovanni, V.; Magrini, U. Experimental Systemic Toxicology of 4'-Epidoxorubicin, a New, Less Cardiotoxic Anthracycline Antitumor Agent. Toxicol. Appl. Pharmacol. 1985, 79 (3), 412–422.

(46) Kratz, F.; Ehling, G.; Kauffmann, H.-M.; Unger, C. Acute and Repeat-Dose Toxicity Studies of the (6-Maleimidocaproyl)Hydrazone Derivative of Doxorubicin (DOXO-EMCH), an Albumin-Binding Prodrug of the Anticancer Agent Doxorubicin. Human & Experimental Toxicology 2007, 26 (1), 19–35. https://doi.org/10.1177/0960327107073825.

(47) Desai, V. G.; Herman, E. H.; Moland, C. L.; Branham, W. S.; Lewis, S. M.; Davis, K. J.; George, N. I.; Lee, T.; Kerr, S.; Fuscoe, J. C. Development of Doxorubicin-Induced Chronic Cardiotoxicity in the B6C3F1 Mouse Model. Toxicology and Applied Pharmacology 2013, 266 (1), 109–121. https://doi.org/10.1016/j.taap.2012.10.025.

(48) El-Mabhouh, A. A.; Mercer, J. R. 188Re-Labelled Gemcitabine/Bisphosphonate (Gem/BP): A Multi-Functional, Bone-Specific Agent as a Potential Treatment for Bone Metastases. Eur J Nucl Med Mol Imaging 2008, 35 (7), 1240–1248. https://doi.org/10.1007/s00259-008-0728-y.

(49) Palma, E.; Correia, J. D. G.; Oliveira, B. L.; Gano, L.; Santos, I. C.; Santos, I. 99mTc(CO)3-Labeled Pamidronate and Alendronate for Bone Imaging. Dalton Trans. 2011, 40 (12), 2787–2796. https://doi.org/10.1039/C0DT01396J.

(50) Xie, H.; Chen, G.; Young, R. N. Design, Synthesis, and Pharmacokinetics of a Bone-Targeting Dual-Action Prodrug for the Treatment of Osteoporosis. J. Med. Chem. 2017, 60 (16), 7012–7028. https://doi.org/10.1021/acs.jmedchem.6b00951.

(51) Souhami, R. L.; Craft, A. W.; Eijken, J. W. V. der; Nooij, M.; Spooner, D.; Bramwell, V. H.; Wierzbicki, R.; Malcolm, A. J.; Kirkpatrick, A.; Uscinska, B. M.; et al. Randomised Trial of Two Regimens of Chemotherapy in Operable Osteosarcoma: A Study of the European Osteosarcoma Intergroup. The Lancet 1997, 350 (9082), 911–917. https://doi.org/10.1016/S0140-6736(97)02307-6.

(52) Jasmin, C.; Allouche, M.; Jude, J. G.; Klein, B.; Thiéry, J. P.; Perdereau, B.; Gongora, R.; Gongora, G.; Mazabraud, A. [An experimental model of osteosarcomas in rats]. Sem Hop 1982, 58 (28–29), 1684–1689.

Table of Contents artwork

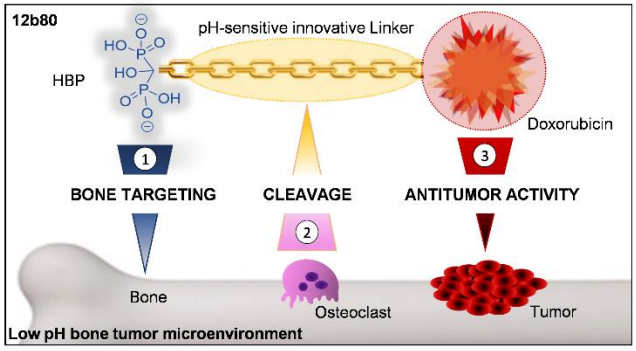

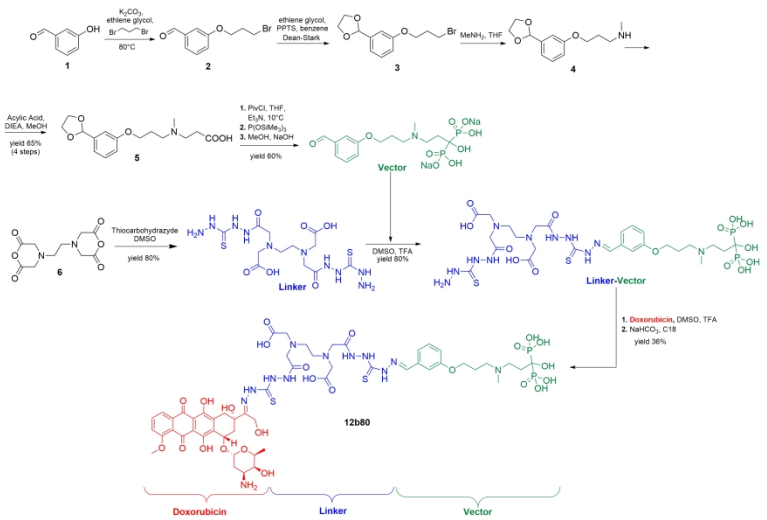

383x219mm (300 x 300 DPI)

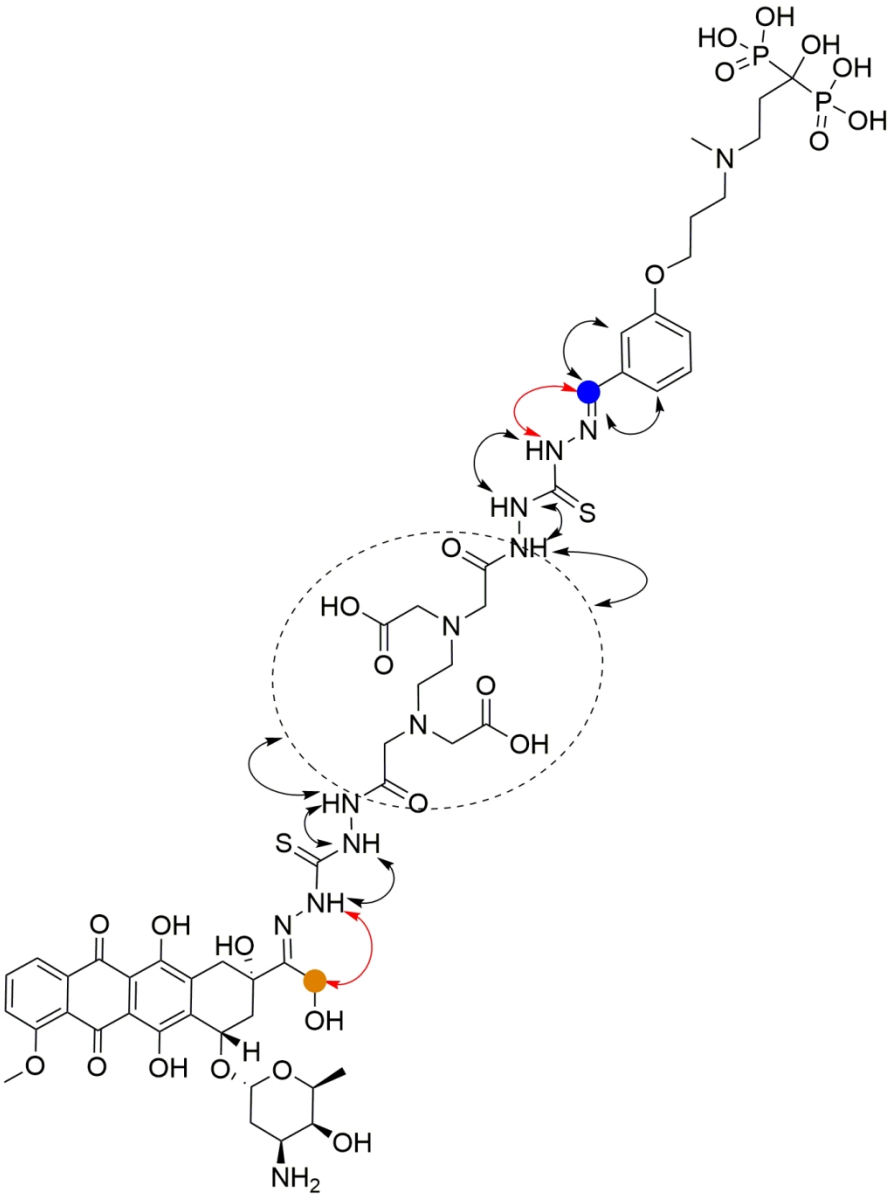

116x156mm (300 x 300 DPI)

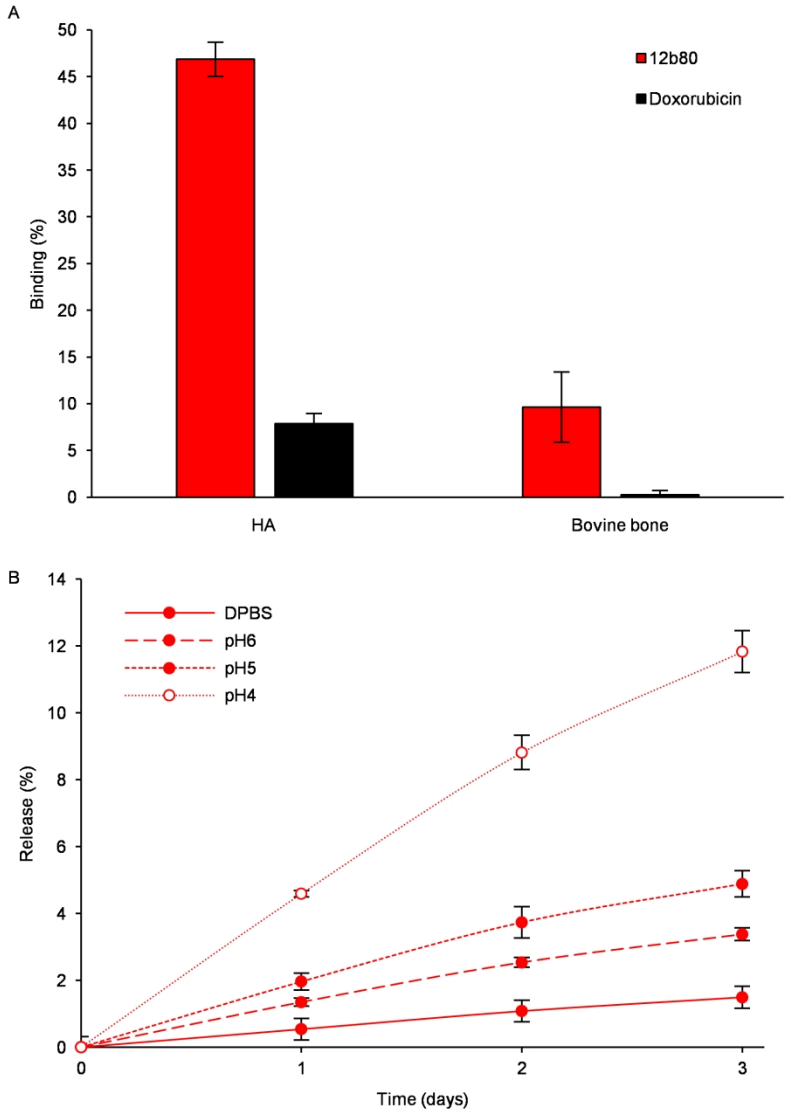

544x750mm (96 x 96 DPI)

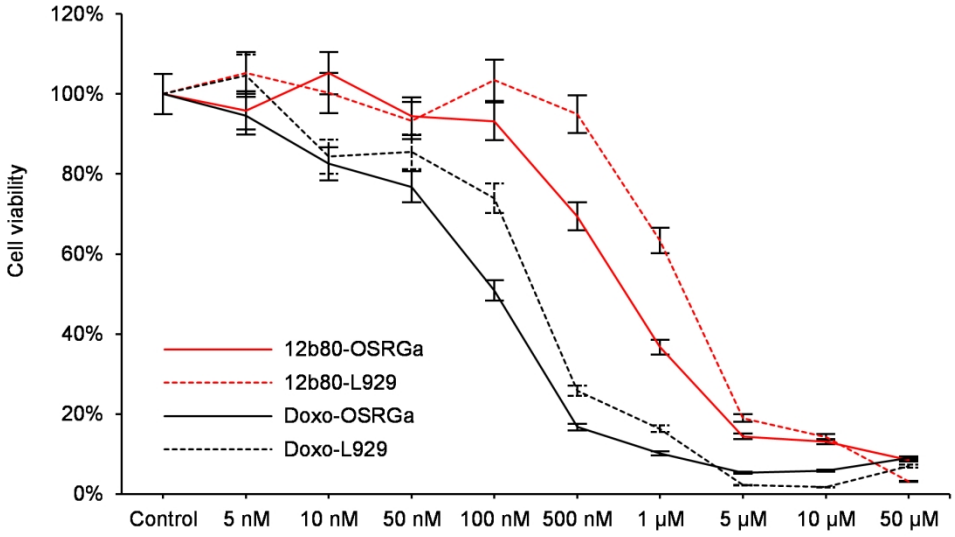

519x298mm (96 x 96 DPI)

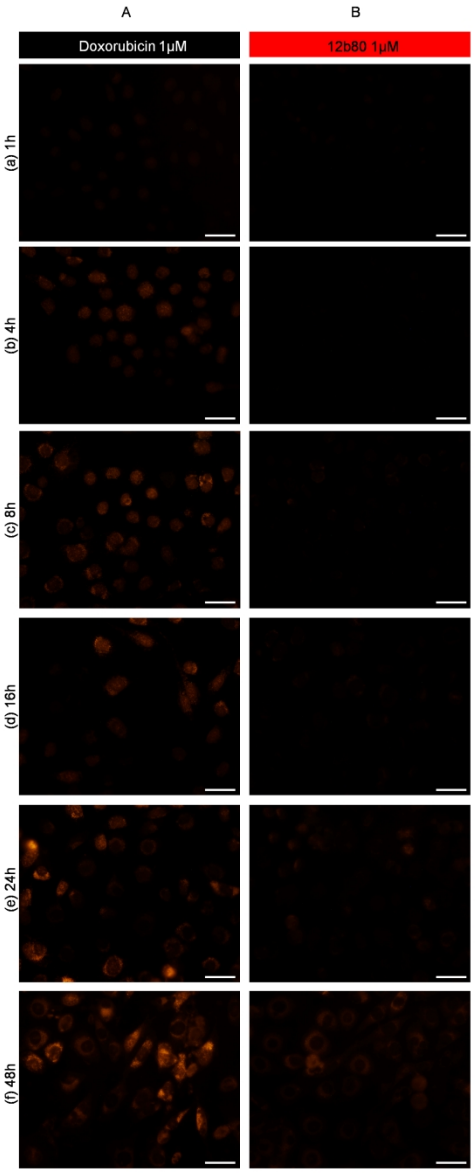

389x913mm (96 x 96 DPI)

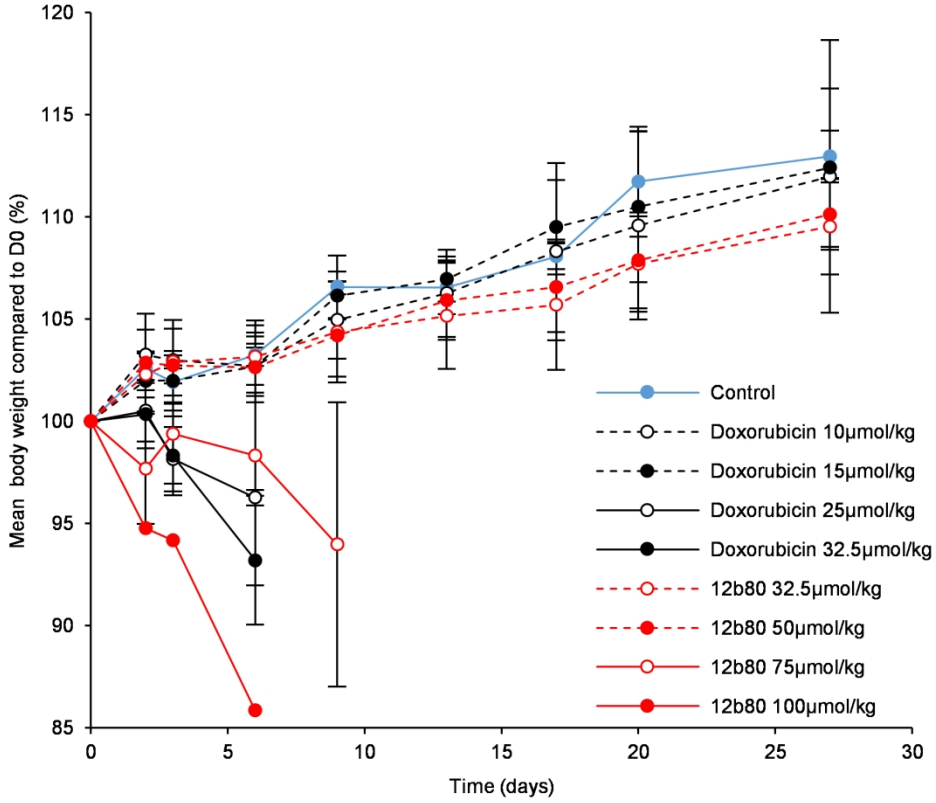

546x480mm (96 x 96 DPI)

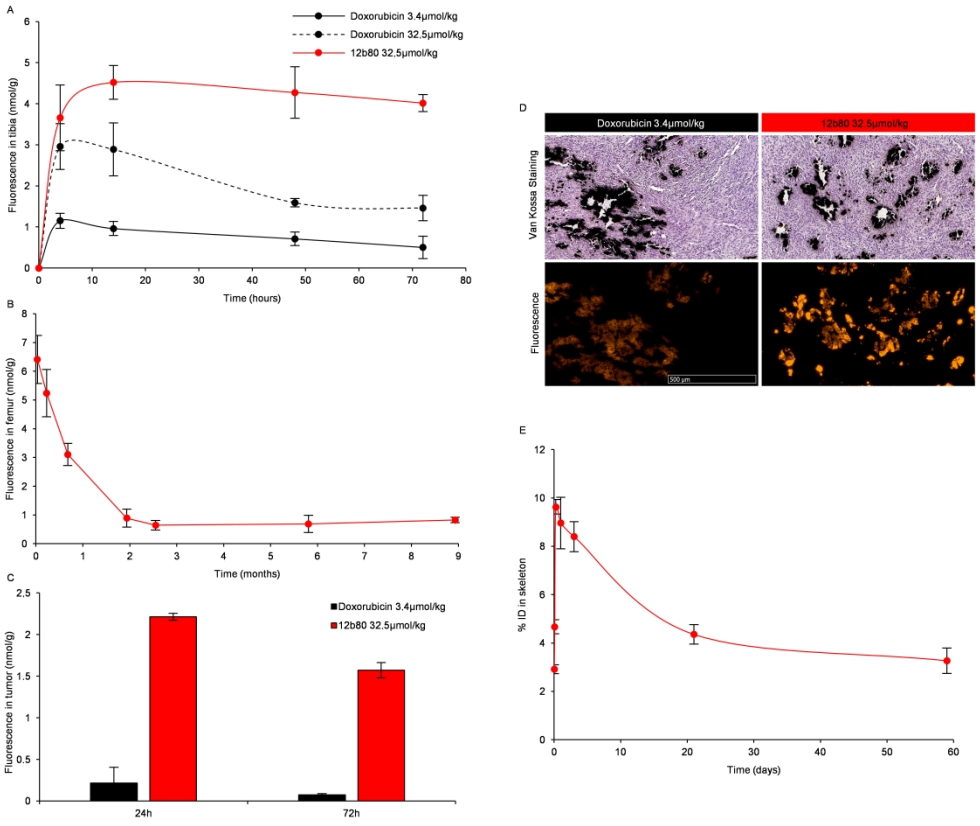

1074x914mm (96 x 96 DPI)

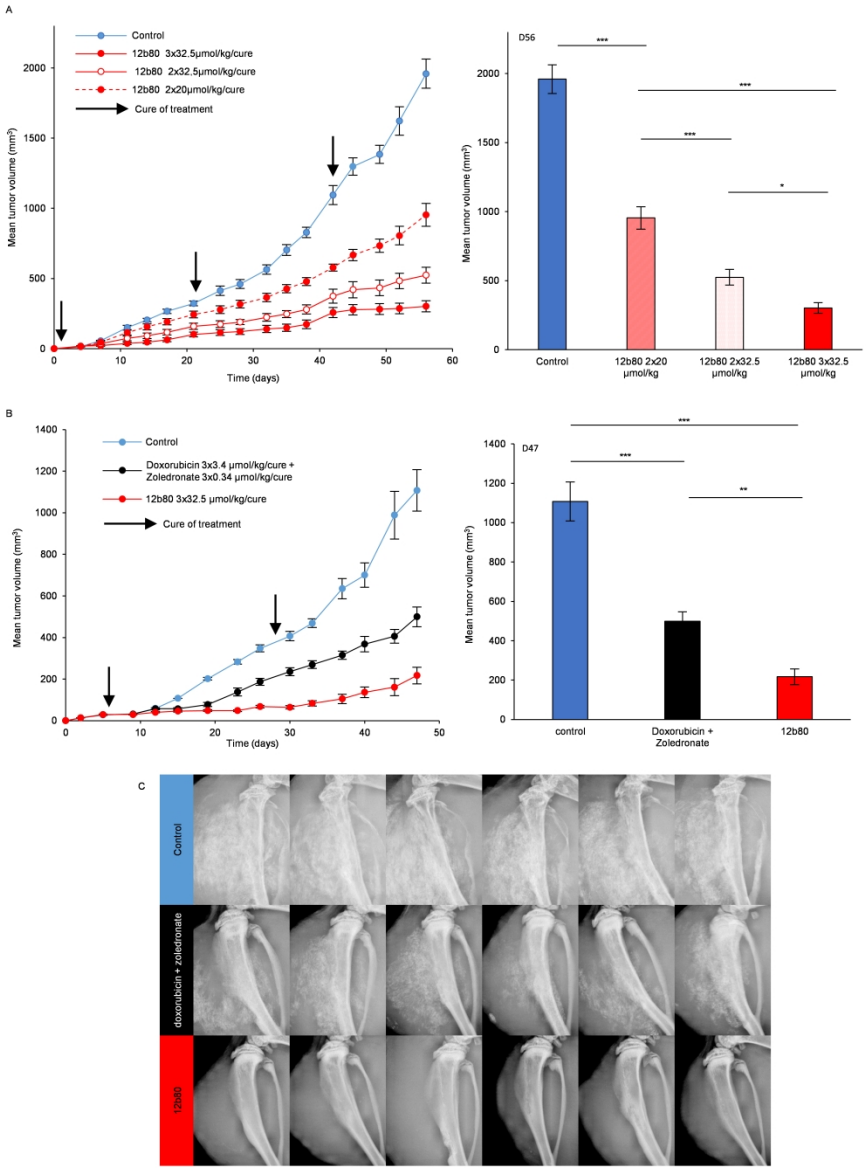

1033x1318mm (96 x 96 DPI)

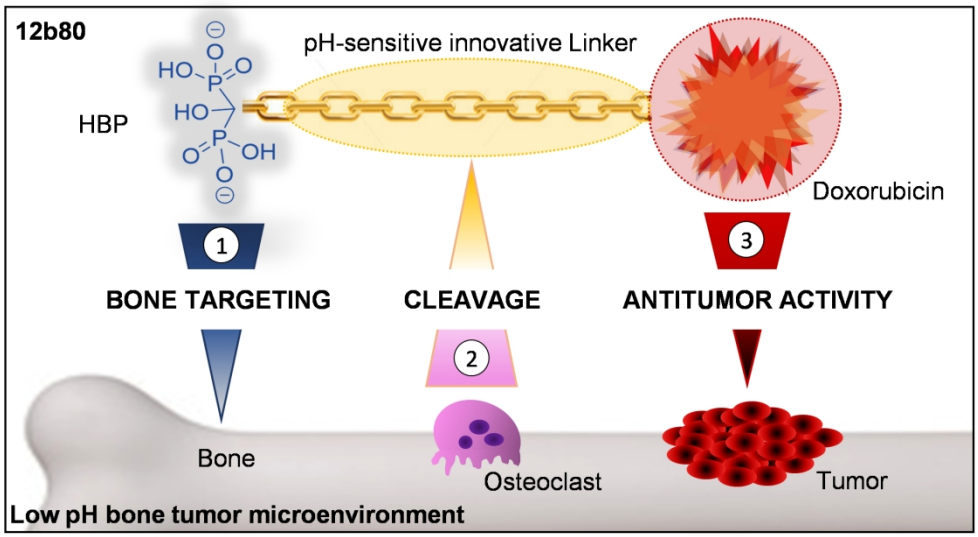

531x299mm (96 x 96 DPI)